Fine particle water and pH in the southeastern United States

Hongyu Guo[1], Lu Xu[2], Aikaterini Bougiatioti[2,8], Kate M. Cerully[2*], Shannon L. Capps[4§], James R. Hite Jr.[1], Annmarie G. Carlton[5], Shan-Hu Lee[6], Michael H. Bergin[1,3], Nga L. Ng[1,2], Athanasios Nenes[1,2,7,†], and Rodney J. Weber[1,†]

[1] School of Earth and Atmospheric Sciences, Georgia Institute of Technology, Atlanta, GA, USA

[2] School of Chemical and Biomolecular Engineering, Georgia Institute of Technology, Atlanta, GA, USA

[3] School of Civil & Environmental Engineering, Georgia Institute of Technology, Atlanta, GA, USA

[4] Office of Research and Development, United States Environmental Protection Agency, Research Triangle Park, NC, USA

[5] Department of Environmental Sciences, Rutgers University, New Brunswick, NJ, USA

[6] College of Public Health, Kent State University, Kent, Ohio, USA

[7] Foundation for Research and Technology, Hellas, Greece

[8] National Technical University of Athens, Athens, Greece

* Now at TSI, Inc., Shoreview, MN, USA

[§] Now at Department of Mechanical Engineering, University of Colorado Boulder, Boulder, CO, USA

[†] Corresponding Author: R. Weber and A. Nenes, (rodney.weber@eas.gatech.edu; athanasios.nenes@gatech.edu)

Abstract

Particle water and pH are predicted using meteorological observations (RH, T), gas/particle composition and thermodynamic modeling (ISORROPIA-II). A comprehensive uncertainty analysis is included, and the model is validated. We investigate mass concentrations of particle water and related particle pH for ambient fine mode aerosols sampled in a relatively remote Alabama forest during the Southern Oxidant and Aerosol Study (SOAS) in summer and at various sites in the southeastern US during different seasons, as part of the Southeastern Center for Air Pollution and Epidemiology (SCAPE) study. Particle water and pH are closely linked; pH is a measure of the particle H^+ aqueous concentration and depends on both the presence of ions and amount of particle liquid water. Levels of particle water, in-turn, are determined through water uptake by both the ionic species and organic compounds. Thermodynamic calculations based on measured ion concentrations can predict both pH and liquid water but may be biased since contributions of organic species to liquid water are not considered. In this study, contributions of both the inorganic and organic fractions to aerosol liquid water were considered and predictions were in good agreement with measured liquid water based on differences in ambient and dry light scattering coefficients (prediction vs. measurement: slope = 0.91, intercept = 0.5 $\mu g\ m^{-3}$, R^2 = 0.75). ISORROPIA-II predictions were confirmed by good agreement between predicted and measured ammonia concentrations (slope = 1.07, intercept = -0.12 $\mu g\ m^{-3}$, R^2 = 0.76). Based on this study, organic species on average contributed 35% to the total water, with a substantially higher contribution (50%) at night. However, not including contributions of organic water had a minor effect on pH (changes pH by 0.15 to 0.23 units), suggesting that predicted pH without consideration of organic water could be sufficient for the purposes of aqueous SOA chemistry. The mean pH predicted in the Alabama forest (SOAS) was 0.94 ± 0.59 (median 0.93). pH diurnal trends followed liquid water and were driven mainly by variability in RH; during SOAS nighttime pH was near 1.5, while daytime pH was near 0.5. pH ranged from 0.5 to 2 in summer and 1 to 3 in the winter at other sites. The systematically low pH levels in the southeast may have important ramifications, such as significantly influencing acid-catalyzed reactions, gas-aerosol partitioning, and mobilization of redox metals and minerals. Particle ion balances or molar ratios, often used to infer pH, do not consider the dissociation state of individual ions or particle liquid water levels and so do not necessarily correlate with particle pH.

Keyword

Particle acidity, pH, particle water, LWC, f(RH), SOA, SOAS, SAS, SCAPE

1 Introduction

The concentration of the hydronium ion (H^+) in aqueous aerosols, or pH, is an important aerosol property that drives many processes related to particle composition and gas-aerosol partitioning (Jang et al., 2002; Meskhidze et al., 2003; Gao et al., 2004; Iinuma et al., 2004; Tolocka et al., 2004; Edney et al., 2005; Czoschke and Jang, 2006; Kleindienst et al., 2006; Surratt et al., 2007; Eddingsaas et al., 2010; Surratt et al., 2010). Measurement of pH is highly challenging and so indirect proxies are often used to represent particle acidity. The most common is an ion balance: the charge balance of measurable cations and anions (excluding the hydronium ion). Although correlated with an acidic (net negative balance) or alkaline (net positive balance) aerosol (Surratt et al., 2007; Tanner et al., 2009; Pathak et al., 2011; Yin et al., 2014), an ion balance cannot be used as a measure of the aerosol concentration of H^+ in air (i.e., moles H^+ per volume of air, denoted hereafter as H^+_{air}). This is due to two factors, first, an ion balance assumes all ions are completely dissociated, but multiple forms are possible, depending on pH (e.g., sulfate can be in the form of H_2SO_4, HSO_4^-, or SO_4^{2-}). Secondly, pH depends on the particle liquid water content (LWC), as pH is the concentration of H^+ in an aqueous solution. LWC can vary considerably over the course of a day and between seasons significantly influencing pH (Seinfeld and Pandis, 2006). Aerosol thermodynamic models, such as ISORROPIA-II (Nenes et al., 1998; Fountoukis and Nenes, 2007) and AIM (Clegg et al., 1998), are able to calculate LWC and particle pH, based on concentrations of various aerosol species, temperature (T), and relative humidity (RH) and offer a more rigorous approach to obtain aerosol pH (Pye et al., 2013). ISORROPIA-II calculates the composition and phase state of an NH_4^+-SO_4^{2-}-NO_3^--Cl^--Na^+-Ca^{2+}-K^+-Mg^{2+}-water inorganic aerosol in thermodynamic equilibrium with water vapor and gas phase precursors. The model has been tested with ambient data to predict acidic or basic compounds, such as $NH_{3(g)}$, NH_4^+, and NO_3^- (Meskhidze et al., 2003; Nowak et al., 2006; Fountoukis et al., 2009; Hennigan et al., 2014).

LWC is a function of RH, particle concentration and composition, and is the most abundant particle-phase species in the atmosphere, at least 2-3 times the total aerosol dry mass on a global average (Pilinis et al., 1995; Liao and Seinfeld, 2005). At 90% RH, the scattering cross-section of an ammonium sulfate particle can increase by a factor of five or more above that of the dry particle, due to large increases in size from water uptake (Malm and Day, 2001). Because of this, LWC is the most important contributor to direct radiative cooling by aerosols (Pilinis et al., 1995), currently thought to be -0.45 Wm^{-2} (-0.95 Wm^{-2} to +0.05 Wm^{-2}) (IPCC, 2013). LWC plays a large role in secondary aerosol formation for inorganic and possibly organic species by providing a large aqueous surface for increased gas uptake and a liquid phase where aqueous phase chemical reactions can result in products of lower vapor pressures than the absorbed gases (Seinfeld and Pandis, 2006; Ervens et al., 2011; Nguyen et al., 2013). In the eastern US, it has been

suggested that the potential for organic gases to partition to LWC is greater than the potential to partition to particle-phase organic matter (Carlton and Turpin, 2013), and partitioning of water soluble organic carbon (WSOC) into the particle phase becomes stronger as RH (i.e., LWC) increases (Hennigan et al., 2008). Thus LWC enhances particle scattering effects directly by increasing particle cross sections (Nemesure et al., 1995) and indirectly by promoting secondary aerosol formation (Ervens et al., 2011; Nguyen et al., 2013).

The behavior of inorganic salts under variable RH is well established both experimentally and theoretically. It is known that dry inorganic salts (or mixtures thereof) exhibit a phase change, called deliquescence, when exposed to RH above a characteristic value. During deliquescence, the dry aerosol spontaneously transforms (at least partially) into an aqueous solution (Tang, 1976; Wexler and Seinfeld, 1991; Tang and Munkelwitz, 1993). In contrast, due to its chemical complexity that evolves with atmospheric aging, the relationship of organics to LWC is not well characterized and requires a parameterized approach (Petters and Kreidenweis, 2007). Relationships between volatility, oxidation level and hygroscopicity are not always straightforward and still remain to be fully understood (Frosch et al., 2011; Villani et al., 2013; Cerully et al., 2014; Hildebrandt Ruiz et al., 2014). Despite the abundance and importance of LWC, it is not routinely measured. Thus typically, particle total mass concentration (that includes liquid water) is often not characterized. In general, LWC is measured by perturbing the in-situ RH. The loss of particle volume when RH is lowered is assumed to be solely due to evaporated water. Approaches for LWC measurements are classified into single particle size probes and bulk size quantification (Sorooshian et al., 2008). Single size particle probes provide more information, i.e., size resolved hygroscopic growth, and usually tend to be slow due to whole size range scanning. In contrast, bulk size measurements quantify the total water amount directly. The LWC measurement presented in this paper by nephelometers is a bulk measurement.

As part of the Southern Oxidant and Aerosol Study (SOAS), we made detailed measurements of particle organic and inorganic composition (Xu et al., 2015), aerosol hygroscopicity (Cerully et al., 2014), and indirect measurements of particle LWC. These data are used to first determine the particle water mass concentrations, which are then utilized in a thermodynamic model for predicting pH. The fine particle LWC and pH data from this analysis are used in our other studies of secondary aerosol formation as part of SOAS and discussed in companion papers to this work (Cerully et al., 2014; Xu et al., 2015).

2 Data collection

2.1 Measurement sites

Aerosol measurements were conducted at the SEARCH Centreville site (CTR; 32.90289 N, 87.24968 W, altitude: 126 m), located in Brent, Alabama, as part of SOAS (Southern Oxidant and Aerosol Study) (http://soas2013.rutgers.edu). SOAS ground measurements were made from June 1st to July 15th in the summer of 2013. CTR is a rural site within a large forested region dominated by biogenic volatile organic compound (VOC) emissions, with minor local anthropogenic emissions and some plumes transported from other locations (coal-fired electrical generating units, urban emissions, biomass burning, mineral dust). It is representative of background conditions in the southeastern US and chosen to investigate biogenic secondary organic aerosol (SOA) formation and its interaction with anthropogenic pollution transported from other locations.

Additional measurements were also made at various sampling sites in and around the metropolitan Atlanta region from May 2012 to December 2012 as part of a large health study; the Southeastern Center for Air Pollution and Epidemiology (SCAPE). A map of all five sites is shown in Figure 1. The SCAPE measurement sites include:

1) A road-side (RS) site (33.775602 N, 84.390957 W), situated within 5m from the interstate highway (I75/85) in midtown Atlanta and chosen to capture fresh traffic emissions;
2) A near-road site (GIT site, 33.779125 N, 84.395797 W), located on the rooftop of the Ford Environmental Science and Technology (EST) building at Georgia Institute of Technology (GIT), Atlanta, roughly 30 to 40 m above ground level, 840 m from the RS site;
3) Jefferson Street (JST) (33.777501 N, 84.416667 W), a central SEARCH site representative of the Atlanta urban environment, located approximately 2000 m west of the GIT site;
4) Yorkville (YRK) (33.928528 N, 85.045483 W), the rural SEARCH pair of JST, situated in an agricultural region approximately 70 km west from the JST, GIT and RS sites.

More information on the SEARCH sites can be found elsewhere (Hansen et al., 2003; Hansen et al., 2006). We first focus on the SOAS campaign data, where a wide range of instrumentation was deployed (http://soas2013.rutgers.edu) to develop a comprehensive method of predicting LWC and pH, as well as assessing their uncertainties. The approach is then applied to the SCAPE site data to provide a broader spatial and temporal assessment of $PM_{2.5}$ pH in the southeastern US.

2.2 Instrumentation

2.2a PILS-IC

$PM_{2.5}$ or PM_1 (particles with aerodynamic diameters < 2.5 or 1.0 μm at ambient conditions) water soluble ions were measured by a Particle-Into-Liquid-Sampler coupled to an Ion Chromatograph (PILS-IC; Metrohm 761 Compact IC). Similar setups are described in previous field studies (Orsini et al., 2003; Liu et al., 2012). Metrosep A Supp-5, 150/4.0 anion column and C 4, 150/4.0 cation column (Metrohm USA, Riverside, FL) were used to separate the PILS liquid sample anions (sulfate, nitrate, chloride, oxalate, acetate, formate) and cations (ammonium, sodium, potassium, calcium, magnesium) at a 20 min duty cycle. The PILS sample ambient air flow rate was 16.8 ± 0.4 L min^{-1}. URG (Chapel Hill, NC) cyclones were used to provide PM cut sizes of $PM_{2.5}$ for the 1st half of field study (June 1 to June 22) and PM_1 for the latter half (June 23 to July 15). Honeycomb acid (phosphoric acid)- and base (sodium carbonate)-coated denuders removed interfering gases before entering the PILS. The sample inlet was ~7 m above ground level and ~4 m long. The sampling line was insulated inside the trailer (typical indoor T was 25 ℃) and less than 1m in length to minimize possible changes in aerosol composition prior to measurement. Periodic 1-hr blank measurements were made every day by placing a HEPA filter (Pall Corp.) on the cyclone inlet. All data were blank corrected. The PILS IC was only deployed for the SOAS study.

2.2b AMS

A High-Resolution Time-of-Flight Aerosol Mass Spectrometer (HR-ToF-AMS, Aerodyne Research Inc., hereafter referred to as "AMS") provided real time, quantitative measurements of the non-refractory components of submicron aerosols (DeCarlo et al., 2006; Canagaratna et al., 2007). In brief, particles were first dried (RH < 20%) and then immediately sampled through an aerodynamic lens into the high vacuum region of the mass spectrometer, then transmitted into a detection chamber where particles impact on a hot surface (600 ℃). Non-refractory species are flash vaporized and then ionized by 70 eV electron impact ionization. The generated ions are extracted into the time-of-flight mass spectrometer. Further details on the AMS setup and data processing can be found in Xu et al. (2015).

2.2c CCNc

The particle hygroscopic parameter, κ (Petters and Kreidenweis, 2007), used to infer the hygroscopic properties (liquid water associated with organics), was obtained from size-resolved CCN measurements from a Droplet Measurement Technologies Continuous-Flow Streamwise Thermal Gradient Cloud Condensation Nuclei counter (CFSTGC, referred to hereafter as CCNc) (Roberts and Nenes, 2005; Lance

et al., 2006). The CCNc exposes aerosols to a known supersaturation, then counts the activated particles that grow rapidly to droplet size. Köhler Theory can be used to parameterize the water phase properties (here, expressed by κ; (Petters and Kreidenweis (2007)) of the organic aerosol, based on the size of particles that form CCN and their composition. A URG (Chapel Hill, NC) PM_1 cyclone was installed for both AMS and CCNc. The details of the CCNc setup and data analysis procedure can be found in Cerully et al. (2014).

2.2d Ambient vs Dry Nephelometers

$PM_{2.5}$ (URG cyclones) aerosol light scattering coefficients (σ_{sp}) were measured online with two different nephelometers (Radiance Research M903) to infer LWC. Both were operated at nominally 3 L min^{-1}. Particle dry scattering was measured with a nephelometer located in the air-conditioned sampling trailer operated with a nafion dryer upstream that maintained an RH of 32 ± 2 % (study mean ± SD, n = 12,464 based on 5-min averages). The other was situated in a small white 3-sided wooden shelter (one side covered by a loose tarp) located a distance away from all buildings to provide a scattering measurement at ambient T and RH. Both $PM_{2.5}$ cut cyclones were located in ambient conditions, and both nephelometers were calibrated by CO_2 prior to the SOAS field campaign. Typical uncertainty is 3% for scattering coefficients (Mitchell et al., 2009). In addition, the nephelometer RH sensors were calibrated by placing the sensors in a closed container above aqueous saturated salt solutions that had reached equilibrium (measurements made in a thermally insulated container after a period of a few hours). Solution temperatures were monitored. Details on the calibration results are provided in the Supplementary Material Section 1. Recorded RH was corrected by the calibration results.

2.3 Determining LWC from nephelometers

Particle water was inferred from the ratio of ambient and dry $PM_{2.5}$ scattering coefficients (σ_{sp}) measured by the two nephelometers (defined here as aerosol hygroscopic growth factor, $f(RH) = \sigma_{sp(ambient)} / \sigma_{sp(dry)}$, where $\sigma_{sp(ambient)}$ and $\sigma_{sp(dry)}$ are particle scattering coefficients at ambient and dry RH conditions, respectively) following the method developed by other investigators (Carrico et al., 1998; Kotchenruther and Hobbs, 1998; Carrico et al., 2000; Malm and Day, 2001; Sheridan et al., 2002; Magi and Hobbs, 2003; Kim et al., 2006). A difference between ambient and dry scattering coefficients is assumed to be caused solely by loss of water. Detailed derivations are provided in the Supplementary Material. $f(RH)$ is related to the particle scattering efficiencies (Q_s) and average particle diameter ($\overline{D_p}$) by;

$$\overline{D_{p,ambient}} = \overline{D_{p,dry}} \sqrt{f(RH)\, \overline{Q_{s,dry}} / \overline{Q_{s,ambient}}} \quad (1)$$

$\overline{Q_{s,ambient}}$, $\overline{D_{p,ambient}}$ are the average scattering efficiency and average particle diameter under ambient conditions, while $\overline{Q_{s,dry}}$, $\overline{D_{p,dry}}$ represent dry conditions. The method is based on fine particle light scattering being mostly due to particles in the accumulation mode and can be related to scattering efficiencies and the diameter of average surface, for both ambient and dry particle size distributions. Assuming that $\overline{Q_{s,ambient}} = \overline{Q_{s,dry}}$ (see Supplementary Material Section 2 for justification and uncertainty analysis), it follows then that;

$$\overline{D_{p,ambient}} = \overline{D_{p,dry}}\sqrt{f(RH)} \quad (2)$$

Since the LWC is equal to the difference between ambient and dry particle volume, we get;

$$f(RH)\_water = [f(RH)^{1.5} - 1]m_p\rho_w/\rho_p \quad (3)$$

where m_p and ρ_p are dry particle mass and density, respectively; ρ_w is water density (constant 1 g cm^{-3} is applied). For SOAS, dry $PM_{2.5}$ mass concentrations were measured continuously by a TEOM (tapered element oscillating microbalance, 1400a, Thermo Fisher Scientific Inc., operated by Atmospheric Research & Analysis Inc., referred to hereafter as ARA). Particle density, ρ_p, was computed from the particle composition, including AMS total organics, ammonium, and sulfate, which accounted for 90% of the measured $PM_{2.5}$ (TEOM) dry mass (SOAS study mean). A typical organic density 1.4 g cm^{-3} is assumed (Turpin and Lim, 2001; King et al., 2007; Engelhart et al., 2008; Kuwata et al., 2012; Cerully et al., 2014), and the density of ammonium sulfate is assumed to be 1.77 g cm^{-3} (Sloane et al., 1991; Stein et al., 1994). ρ_p was calculated to be 1.49 ± 0.04 g cm^{-3} (n = 4,393) using mass fractions (ε):

$$\rho_p = \frac{1}{\varepsilon(NH_4^+ + SO_4^{2-})/1.77 + \varepsilon\,(Organics)/1.4}\ (g\ cm^{-3}) \quad (4)$$

The time-resolved composition data shows that dry particle density did not have a significant diurnal variability (±2.7%, SD/mean, Supplementary Material Figure S2). In the following we refer to the particle water calculated by this method as $f(RH)$_water. The uncertainty of $f(RH)$_water is estimated to be 15%, mainly caused by the calculation of $\overline{Q_{s,ambient}}/\overline{Q_{s,dry}}$ (LWC error of 10% from assuming $\overline{Q_{s,ambient}}/\overline{Q_{s,dry}}$ = 1, see Supplementary Material), m_p (10%), $\sigma_{sp(ambient)}$ / $\sigma_{sp(dry)}$ (4.2%) (uncertainty for a single σ_{sp} measurement is 3%, Mitchell et al. (2009)), and ρ_p (2.7%). Note that LWC error depends on RH, and for SOAS average aerosol composition could increase to 21% for RH > 90% (Supplementary Material Figure S6).

3 Modeling Methods: Predicting LWC and pH from aerosol composition

In most studies, such as SCAPE, particle water was not measured and must be determined based on aerosol composition. Both inorganic and organic components contribute to uptake of water vapor, establishing equilibrium for the ambient RH and T conditions. Thus, LWC is controlled by

meteorological conditions and also by aerosol concentration and composition. Thermodynamic models, such as ISORROPIA-II, have been extensively used to predict LWC due to inorganic aerosol components (Fountoukis and Nenes, 2007). Contributions to LWC by organic components are typically based on an aerosol hygroscopicity parameter, κ, which is determined by CCN data. Here we refer to particle water associated with inorganics and organics as W_i and W_o, respectively. Total particle water ($W_i + W_o$) is taken as the sum of water associated with individual aerosol chemical components (sum of ions and lumped organics) based on Zdanovskii-Stokes-Robinson (ZSR) relationship (Zdanovskii, 1936; Stokes and Robinson, 1966), with the assumption that the particles are internally mixed. The assumptions made in our analysis were discussed in Section 3.4.

3.1 LWC from inorganic species

Particle water associated with inorganic species (W_i) were predicted by ISORROPIA-II (Nenes et al., 1998; Fountoukis and Nenes, 2007). ISORROPIA-II calculates the composition and phase state of a K^+-Ca^{2+}-Mg^{2+}-NH_4^+-Na^+-SO_4^{2-}-NO_3^--Cl^--water inorganic aerosol in thermodynamic equilibrium with gas phase precursors. Chemical and meteorological data are necessary inputs. For our analysis at CTR, the inputs to ISORROPIA-II are the inorganic ions measured by the IC or AMS, RH measured by the outside nephelometer, and temperature from the SEARCH site (ARA) meteorological data.

3.2 LWC from organic fraction

To determine the contributions to particle water by W_o, in SOAS the organic hygroscopicity parameter (κ_{org}) was calculated based on the observed CCN activities of the organic fraction (Cerully et al., 2014). In the following analysis diurnal three-hour running averages are used in the calculation. (Diurnal plot is included in the Supplementary Material as Figure S7). W_o is calculated using the following equation (Petters and Kreidenweis, 2007).

$$W_o = \frac{m_{org}\rho_w}{\rho_{org}} \frac{\kappa_{org}}{\left({}^{1}/_{RH} - 1\right)} \quad (5)$$

where m_{org} is the organic mass concentration from AMS (Xu et al., 2015), ρ_w is water density, and a typical organic density (ρ_{org}) of 1.4 g cm^{-3} is used (Turpin and Lim, 2001; King et al., 2007; Engelhart et al., 2008; Kuwata et al., 2012; Cerully et al., 2014).

3.3 pH prediction

The thermodynamic model, ISORROPIA-II (Fountoukis and Nenes, 2007), calculates the equilibrium particle hydronium ion concentration per volume air (H^+_{air}), which along with the LWC is then used to

predict particle pH. To correct for the LWC associated with the organic aerosol (not considered in ISORROPIA-II), we recalculate pH by considering H^+_{air} and total predicted water (W_i and W_o). The modeled concentrations are μg m^{-3} air for H^+_{air} and LWC. The pH is then,

$$pH = -\log_{10} H^+_{aq} = -\log_{10} \frac{1000 H^+_{air}}{W_i + W_o} \quad (6)$$

where H^+_{aq} (mol L^{-1}) is hydronium concentration in an aqueous solution. H^+_{air} and W_i are the output of ISORROPIA-II based on input of water soluble ions, RH, and T. H^+_{aq} is H^+_{air} divided by the LWC, and so including W_o decreases H^+_{aq} by a factor of $W_o/(W_i+W_o)$, relative to only considering W_i.

ISORROPIA-II has been tested in previous field campaigns where a suite of both gas and particle components were measured (Nowak et al., 2006; Fountoukis et al., 2009). The model was able to predict the equilibrium partitioning of ammonia (Nowak et al., 2006) in Atlanta and nitric acid (Fountoukis et al., 2009) in Mexico City within measurement uncertainty. For instance, $NH_{3(g)}$, NH_4^+, $HNO_{3(g)}$, and NO_3^- were within 10%, 20%, 80%, and 20% of measurements (Fountoukis et al., 2009). In this study, ISORROPIA-II was run in the "Forward mode" for metastable aerosol. Forward mode calculates the equilibrium partitioning given the total concentration of various species (gas + particle) together with RH and T as input. Reverse mode involves predicting the thermodynamic composition based only on the aerosol composition. Here we use the Forward mode with just aerosol phase data input because it is less sensitive to measurement error than the Reverse mode (Hennigan et al., 2014). The W_i prediction remains the same (Reverse vs Forward: slope = 0.993, intercept = -0.005 μg m^{-3}, and R^2 = 0.99) no matter which approach is used. Gas phase input does have an important impact on the H^+_{air} calculation. ISORROPIA-II was tested with ammonia partitioning, which is discussed in more detail below. Here it is noted that we found that further constraining ISORROPIA-II with measured $NH_{3(g)}$ (You et al., 2014) resulted in a pH increase of 0.8 at CTR and that the predicted $NH_{3(g)}$ matched the measured $NH_{3(g)}$ well (slope = 1.07, intercept = -0.12 μg m^{-3}, R^2 = 0.76). This also confirms that ISORROPIA-II predicts the pH in the ambient aerosol with reasonable accuracy, as inputting the total (gas + aerosol) ammonium results in predictions that agree with those observed. This is also in agreement with findings of Hennigan et al. (2014) and Fountoukis et al. (2009), both of whom found that ISORROPIA-II reproduced the partitioning of ammonia and inorganic nitrate in Mexico City during the MILARGO campaign.

3.4 Assumptions

In the following analysis we use bulk properties and do not consider variability in parameters with particle size. Particulate organic and inorganic species are assumed to be internally mixed in the liquid phase due to the high RH (74 ± 16%) typical of this study and because a large fraction of the ambient

aerosol organic component is from isoprene SOA (Xu et al., 2015), which are liquids at RH ≥ 60% (Song et al., 2015). Particle liquid phase separations are not considered, although they have been measured in bulk extracts of aerosols from the southeast (You et al., 2012). It is reported that liquid-liquid phase separation can occur when the O:C ratio of the organic material is ≤ 0.5. More experiments showed that it is possible to have phase separation for O:C ≤ 0.7, but not for O:C ≥ 0.8 (Bertram et al., 2011; Song et al., 2012; You et al., 2013). SOAS average O:C = 0.75 (± 0.12) is in the transition between these two regimes. According to Figure 2 in Bertram et al. (2011), at RH typically > 60% and organic:sulfate mass ratio >1, it is not possible to have phase separation, which is the case for our sampling sites. Based on our basic assumption of no liquid-liquid phase separation, pH is considered to be homogeneous in a single particle. However, separated phases would likely have different pHs if liquid-liquid phase separation occurs. In that case, pH should be calculated based on the amounts of water and H^+_{air} in each phase. Gas-particle phase partitioning will change accordingly, due to these separated phases. There are models that are set up to calculate these thermodynamics (e.g., AIOMFAC), but none is yet able to address the compositional complexity of ambient SOA. (Zuend et al., 2010; Zuend and Seinfeld, 2012) Although it is often true that non-ideal interactions between organic and inorganic species exist, good agreement between measured particle water and ammonia partitioning to predictions using the bulk properties (discussed below) suggests these assumptions are reasonable.

4 Results

4.1 Overall summary of meteorology and PM composition at SOAS and SCAPE sites

For the SOAS study period, mean T and RH were 25 ± 3 ℃ and 74 ± 16 % (mean ± SD), respectively. This resulted in a $f(RH)$_water level of 4.5 ± 3.8 μg m^{-3}, with a maximum value of 28.4 μg m^{-3}. In comparison, SOAS mean dry $PM_{2.5}$ mass was 7.7 ± 4.6 μg m^{-3}, implying that the fine aerosols were roughly composed of 37% water, on average. Mean T and RH for SCAPE sites are listed in Table 3. Summer T means were all above 21℃, including CTR. RH means were all high (> 60%) for summer and winter, which is typical for the southeastern US.

Of the sites in the southeastern US discussed in this paper, CTR was the least influenced by anthropogenic emissions having the lowest black carbon (BC) concentrations (measured by a MAAP, Thermo Scientific, model 5012). At CTR, the mean BC = 0.3 ± 0.2 μg m^{-3} (± SD), whereas mean BC concentrations at the other rural site (YRK) was 0.4 μg m^{-3}. The representative Atlanta site (JST) BC was on average 0.7 μg m^{-3}, and higher for sites closer to roadways, 1.0 μg m^{-3} (GIT) and 2.0 μg m^{-3} (RS).

A more comprehensive suite of ions will provide a better prediction of W_i. However, in the southeastern US, inorganic ions are currently dominated by sulfate and ammonium. During SOAS, the PILS-IC provided a more comprehensive and accurate measurement of water-soluble ions than AMS, which measured only non-refractory sulfate, ammonium, nitrate, and chloride. Refractory, but water soluble ions, such as sodium and associated chloride, and crustal elements including calcium, potassium, and magnesium were present in PM_1, but in very low concentrations. Contributions of these ions are more important in $PM_{2.5}$ than for PM_1, which tend to reduce aerosol acidity. For instance, Na^+ has a significantly higher mean in $PM_{2.5}$ at 0.056 μg m^{-3} (1st half of SOAS study) than 0.001 μg m^{-3} in PM_1 (2nd half of SOAS study). Four, one day-long, dust events (06/12, 06/13, 06/16, and 06/21) in the SOAS data set have been excluded from this analysis as assumptions relating to internal mixing of $PM_{2.5}$ components are less valid in these cases. Excluding these days, the mean Na^+ in $PM_{2.5}$ drops to 0.024 μg m^{-3}.

If the fraction of the refractory ions (e.g., Na^+, K^+, Ca^{2+}, Mg^{2+}) is negligible compared to the SO_4 (Note, SO_4 stands for sulfate in all its possible forms, from free to completely dissociated), NH_4^+, and NO_3^-, the AMS data sufficiently constrains particle composition for thermodynamic calculations; this apparently is the case for most of the time in the southeast (Supplementary Material Section 4). For PM_1 SO_4 and NH_4^+, AMS and PILS-IC were in good agreement (SO_4 slopes within 20 %, $R^2 = 0.90$; NH_4^+ within 1%, $R^2 = 0.81$). Similar agreement was also found for AMS PM_1 SO_4 and NH_4^+ versus PILS-IC $PM_{2.5}$ SO_4 and NH_4^+. (See Figure 2 for comparison of complete data set). These data indicate little SO_4 and NH_4^+ between the 1.0 and 2.5 μm size range ($PM_{2.5} - PM_1$). Because of the agreement between these dominant ions, ISORROPIA-II predicted W_i for all ions measured with the PILS-IC throughout the study (includes both PM_1 and $PM_{2.5}$) agreed with W_i based on AMS inorganic species (i.e., only ammonium and sulfate) having an orthogonal slope of 1.18, Figure 2c.

4.2 Results from the SOAS Centreville site

4.2a LWC, pH and ion balances at Centreville

The diurnal variation of LWC contributed by W_i and W_o, along with total measured water, ambient T, RH, and solar radiation at CTR is shown in Figure 3. Predicted and measured LWC trends were in good overall agreement, although the largest discrepancy was observed during the daytime when the LWC level was low and more difficult to measure and accurately predict. Nighttime RH median values were between 85% and 90% and resulted in significant water uptake that reached a peak just after sunrise near 7:30 am (local time). The dramatic peak in LWC starting at roughly 5:00 am, reaching a maximum between 7:30 and 8:00 am is likely due to RH increasing above 90%, at which point uptake of water rapidly increases with increasing RH. The similar rapid hygroscopic growth before sunrise was also

observed at GIT, RS, and JST (Nov) (Figure 11). After sunrise, rising temperatures led to a rapid drop in RH, resulting in rapid loss of particle water. LWC reached lowest levels (~2 μg m^{-3}) in the afternoon, only 20% of the peak value. W_o varied more than W_i diurnally; W_o max/min ratio was 13.1 compared to 4.1 for W_i.

At CTR, the aerosol was highly acidic, with predicted mean pH = 0.94 ±0.59 (±SD). The minimum and maximum pH were -0.94 and 2.23 respectively, and pH varied by approximately 1 on average throughout the day (Figure 4a). That is, the H^+_{air}/LWC ratio increased by a factor of 10 from night to day. LWC max/min ratio was 5, whereas H^+_{air} diurnal variation was significantly less (Figure 4b), indicating that the diurnal pattern in pH was mainly driven by particle water dilution. This is further demonstrated in Figure 4d, which shows the diurnal variation in the NH_4^+/SO_4^{2-} molar ratio (the main ions driving pH), with only slightly lower ratios during the day. The study mean (±SD) NH_4^+/SO_4^{2-} molar ratio was 1.4 (±0.5). As LWC is mainly controlled by RH and temperature, the pH diurnal variation was thus largely driven by meteorological conditions, not aerosol composition.

In part, because of the diurnal variation of LWC, a simple ion balance or NH_4^+/SO_4^{2-} molar ratio or per volume air concentration of aerosol hydronium ion (H^+_{air}) alone cannot be used as a proxy for pH in the particle. Figure 5a shows a weak inverse correlation (R^2 = 0.36) between ion balance and pH. An ion balance of an aerosol is usually calculated as follows (in unit of nmol equivalence m^{-3}), for a NH_4^+-Na^+-SO_4^{2-}-NO_3^--Cl^--water inorganic aerosol.

$$Ion\ Balance = \frac{[SO_4^{2-}]}{48} + \frac{[NO_3^-]}{62} + \frac{[Cl^-]}{35.5} - \frac{[NH_4^+]}{18} - \frac{[Na^+]}{23} \quad (7)$$

where $[SO_4^{2-}]$, $[NO_3^-]$, $[Cl^-]$, $[NH_4^+]$, and $[Na^+]$ are concentrations of these ions in units of g m^{-3}. An ion balance is also a bad indicator of pH because it poorly predicts the aerosol concentration of H^+_{air}. An ion balance assumes all ions are completely dissociated, but multiple forms are possible, depending on pH (e.g., sulfate can be in the form of H_2SO_4, HSO_4^-, or SO_4^{2-}). For example, if aerosol sulfate remains in the free form of H_2SO_4, it does not add protons. Thus, an ion balance usually overestimates protons and is only moderately correlated with H^+_{air} (Figure 5b).

LWC uncertainty:

In estimating the water uncertainty, we consider W_i and W_o separately. The uncertainty of W_i is estimated by propagating the measurement uncertainty of ions and RH through the ISORROPIA-II thermodynamic model by finite perturbations about the model base state. Uncertainties of ions were estimated by difference between IC-ions and AMS-ions, as well as PILS-IC measurement uncertainty (Table 2). Na^+ is excluded because it is not measured by the AMS. PILS-IC instrumental uncertainty is estimated to be 15%

from the variability in standards (variability is calibration slopes), blanks, sample airflow rate, and liquid flow rate (one SD). The total ion uncertainties are listed in Table 2. SO_4 has a higher uncertainty, at 25%, than the rest, which are at 15%. These combined uncertainties lead to an W_i uncertainty of 25% (Figure 6), which is the same as the SO_4 uncertainty. SO_4, one of the most hygroscopic ions (Petters and Kreidenweis, 2007), controls W_i uptake.

For the SOAS study, the RH probe in the ambient nephelometer (Humitter 50U, VAISALA Inc.) has a stated maximum uncertainty of 5% at RH = 90%. RH biases with respect to environment conditions can also occur due to placement of the probe. Based on RH comparisons between ARA, Rutgers (Nguyen et al., 2014), and the Georgia Tech instrumentation, a systematic bias as large as 10% is found. Given this, we consider an RH probe factory uncertainty (5%) as a typical value and inter-comparison difference (10%) as an extreme condition. In this analysis, RH was adjusted by ±5% and ±10% and W_i recalculated (Figure 7). A ±5% perturbation in RH leads to a 91% (slope – 1) error for 5% perturbation above the measured value (1.05RH) and 29% error for a perturbation below the measured value (0.95RH). We take 60% as average uncertainty. Higher uncertainty is introduced with increasing RH, owing to the exponential growth of LWC with RH and results in the asymmetric LWC uncertainty. Combining W_i uncertainty from ions (25%) and RH (60%), the overall uncertainty is calculated as 65%.

The uncertainty sources for W_o are κ_{org}, ρ_s, m_s, and RH (Equation 5). The uncertainties of these parameters are estimated to be 26% (details can be found in Supplementary Material Section 3), 10%, 20%, and 5% (from above), respectively. In summary, the overall uncertainty of W_o is 35%.

The total uncertainty of LWC can be expressed as a sum of W_i and W_o uncertainties, where ε_i is the mass fraction. ε_{W_o} was found to be 36% and ε_{W_i} was 64%.

$$\frac{\delta_{LWC}}{LWC} = \sqrt{\left(\varepsilon_{W_i}\frac{\delta_{W_i}}{W_i}\right)^2 + \left(\varepsilon_{W_o}\frac{\delta_{W_o}}{W_o}\right)^2} \quad (8)$$

Given the above, $\frac{\delta_{LWC}}{LWC}$ is 43%. This method of assessing predicted LWC uncertainty can be applied to SCAPE sites as well. The specific predicted LWC at SCAPE sites were calculated and are listed in Table 3. W_i uncertainty associated with ions is the same as noted above, 25%, because it is estimated by PILS-IC and AMS differences. Similar uncertainties in W_i at the SCAPE sites are expected if RH uncertainties are similar at all sites.

pH uncertainty:

As pH is based on H^+_{air} and LWC, the uncertainty of pH can be estimated from these two parameters. We applied the adjoint model of ISORROPIA, ANISORROPIA (Capps et al., 2012), to quantify the sensitivity of predicted H^+_{air} to the input aerosol species at the conditions of the thermodynamic calculations. pH uncertainty resulting from aerosol composition is then determined by propagating the input parameter uncertainties, using ANISORROPIA sensitivities, to the corresponding H^+_{air} and pH uncertainty.

We now assess how pH of $PM_{2.5}$ is affected by using an incomplete measurement of ionic species by comparing the pH predicted based on the more complete suite of ions measured by the PILS-IC versus the AMS, during SOAS. Sensitivities of aerosol species to H^+_{air} were calculated by ANISORROPIA with PILS-IC data and presented as partial derivatives (Table 2). Higher sensitivity values imply the inorganic ion is more important for ion balance. In the SOAS study, H^+_{air} is most sensitive to SO_4, and then NH_4^+, as they were the major ions. Uncertainties of ions were estimated by the difference between IC-ions and AMS-ions, as well as PILS-IC measurement uncertainty. Since Na^+ is not measured by AMS, we cannot estimate the difference between PILS-IC and AMS. The loadings and sensitivities of NO_3^- and Cl^- were very low, so they are assumed not to contribute much to $\frac{\delta_{H^+_{air}}}{H^+_{air}}$. Given this, $\frac{\delta_{H^+_{air}}}{H^+_{air}}$ is determined by;

$$\frac{\delta_{H^+_{air}}}{H^+_{air}} = \sqrt[2]{\left(\frac{\partial H^+_{air}}{\partial SO_4}\frac{\delta_{SO_4}}{SO_4}\right)^2 + \left(\frac{\partial H^+_{air}}{\partial NH_4^+}\frac{\delta_{NH_4^+}}{NH_4^+}\right)^2 + \left(\frac{\partial H^+_{air}}{\partial Na^+}\frac{\delta_{Na^+}}{Na^+}\right)^2} \quad (9)$$

Based on the input for Equation 9 (Table 2), $\frac{\delta_{H^+_{air}}}{H^+_{air}}$ is estimated as 14%. LWC is most sensitive to RH fluctuations, so it is considered the main driver of LWC uncertainty in the pH calculation. As discussed, we artificially adjusted RH by ±5% and ±10% (10% is considered an extreme condition). H^+_{air}, W_i, W_o, as well as pH were all recalculated using 90%, 95%, 105%, and 110% of the actual measured RH. RH+5% and RH-5% lead to 12% and 6% variation in pH based on orthogonal regression slopes, respectively (Figure 8). RH-10% results in only 10% variation, however, RH+10% results in a 45% variation, and the coefficient of determination (R^2) between pH calculated based on RH+10% and original RH drops to only 0.78, while for all other cases $R^2 > 0.96$. The disproportionately large effect of the positive uncertainty is caused by the exponential increase of LWC with RH, as RH reaches high levels (>90%). Assuming the stated manufacturer uncertainty (5%) for our RH uncertainty, pH uncertainty is estimated to be 6%-12%. We take 12% as $\frac{\partial pH}{\partial LWC}\delta_{LWC}$ for further calculations.

SO_4 was found to contribute the most to $\frac{\delta_{H^+_{air}}}{H^+_{air}}$. NH_4^+ and Na^+ followed. SO_4 and NH_4^+ are the two most abundant inorganic components in aerosols and controlling aerosol acidity. Finally, the total pH uncertainty is the combination of LWC and the uncertainty associated with H^+_{air}, which is computed from the definition of pH (Equation 6).

$$\frac{\delta_{pH}}{pH} = \sqrt[2]{\left(\frac{\partial pH}{\partial H^+_{air}}\delta_{H^+_{air}}\right)^2 + \left(\frac{\partial pH}{\partial LWC}\delta_{LWC}\right)^2} \quad (10)$$

where $\frac{\partial pH}{\partial H^+_{air}}$ can be derived from Equation (6) as

$$\frac{\partial pH}{\partial H^+_{air}} = -\frac{1}{2.303}\frac{1}{\frac{H^+_{air}}{LWC}}\frac{1}{LWC} = -\frac{1}{2.303}\frac{1}{H^+_{air}} \quad (11)$$

From Equation 9 and the uncertainties of H^+_{air} and LWC (Equation 7 and 8), we estimate the pH uncertainty for the SOAS dataset to be 13% (based on the specific uncertainties considering here). pH uncertainties at SCAPE sites were also assessed via this method. As discussed above, $\frac{\delta_{H^+_{air}}}{H^+_{air}}$ was found to be 14% for the SOAS study, due to IC and AMS data set differences and PILS-IC instrumental uncertainty. This same uncertainty is applied to SCAPE, where no PILS-IC data were available. Because aerosol composition at all sites is similar, based on filter IC analysis (Supplementary Material Figure S8), similar sensitivities of H^+_{air} to ions are expected. However, actual uncertainty for each sampling period is possibly higher due to higher loadings of refractory ions at SCAPE sites due to contributions from urban emissions. Refractory ions not measured by the AMS (i.e. Na^+, K^+, Ca^{2+}, Mg^{2+}), have a minor effect on predicting LWC, but may have an important effect on pH (e.g., result in higher pH) in locations where they could substantially contribute to the overall ion balance.

4.2b Model validation: Prediction of liquid water

Several LWC measurements were made at CTR during SOAS. In addition to $f(RH)$_water (4.5 ± 3.8 μg m^{-3}), particle water was quantified with a Semi-volatile Differential Mobility Analyzer (SVDMA). With this method, a SOAS study mean particle water concentration of 4.3 ± 3.7 μg m^{-3} (± STD) was obtained (Nguyen et al., 2014). The orthogonal regression between these two measurements (SVDMA water vs $f(RH)$_water) has slope = 0.91, intercept = -0.0 μg m^{-3}, R^2 = 0.35. Differences could be caused by differences in size-resolved composition (particle composition beyond PM_1 that contributes LWC; SVDMA scans up to 1.1 μm, while $f(RH)$_water is based on $PM_{2.5}$), instrument sample heating (i.e., the degree to which the instrument was close to ambient conditions, especially when ambient RH was high, and most sensitive to slight T differences), and differences in RH probe calibrations.

CTR predicted total LWC, (W_i + W_o), was 5.1 ± 3.8 μg m^{-3} and agreed well with $f(RH)$_water. The total predicted water was highly correlated and on average within 10% of the measured water, with slope = 0.91, intercept = 0.5 μg m^{-3}, R^2 = 0.75 (see Figure 9). Since excluding refractory ions (Section 4.1) and not considering gas phase species in the ISORROPIA-II calculations do not significantly affect the LWC prediction, its comparison across sites is less uncertain than pH.

4.2c Model validation: Prediction of pH

ISORROPIA-II calculations of pH at CTR for the SOAS study were evaluated by comparing measured and predicted $NH_{3(g)}$. Although NH_4^+ and $NH_{3(g)}$, along with other aerosol components, are input into the model, comparing ambient NH_4^+ and $NH_{3(g)}$ to model predictions is not a circular analyses. For each observed data point, the model calculates total ammonia from the NH_4^+ and $NH_{3(g)}$ input, and then calculates the gas-particle ammonia partitioning assuming equilibrium. There are also other various assumptions/limitations associated with the model. Figure 10 shows the SOAS study time series of measured and predicted $NH_{3(g)}$ and the fraction of ammonia in the gas phase ($NH_{3(g)}$ / ($NH_{3(g)}$ + NH_4^+). Measured and predicted $NH_{3(g)}$ are in good agreement. Periods when almost all ammonia was in the gas phase (ratio near 1) are related to precipitation events (06/10, 06/24, 06/28, 07/03, 07/04) when aerosol concentrations were very low. Not including these events, the study mean (± SD) fraction ammonia in the gas phase was 0.41 (± 0.16) (median value is also 0.41). These results provide confidence in ISORROPIA-II calculations of particle pH, and demonstrate the utility of including both measurements of particle and gas phases in these types of studies.

When gas data are not available, pH predictions are not as accurate (Hennigan et al., 2014). Running ISORROPIA-II in the forward mode, but with only aerosol concentrations as input, may result in a bias in predicted pH due to repartitioning of ammonia in the model. In the southeast, where pH is largely driven by SO_4 and NH_4^+, the aerosol NH_4^+ input will be partitioned in the model between gas and particle phases to establish equilibrium. Sulfate repartitioning does not occur since it is non-volatile. Thus, NH_4^+ will be lost from the particle and a lower pH predicted. At CTR ammonia partitioning has been included in all model runs, but as no $NH_{3(g)}$ was available for SCAPE. Assuming the average $NH_{3(g)}/NH_4^+$ ratio from CTR applies to all SCAPE sites to estimate $NH_{3(g)}$, along with measured particle composition at each site, we got pH increases ranging from 0.87 to 1.38. In the following, all pHs reported for SCAPE are corrected for this bias (i.e., pHs are increased by 1 to simplify the correction). Note that ammonia partitioning does not significantly affect the LWC prediction (W_i predicted without $NH_{3(g)}$ vs W_i predicted with $NH_{3(g)}$: slope = 1.00, intercept = -0.01 μg m^{-3}, R^2 = 0.98).

4.3 LWC and pH at other sites in the southeast (SCAPE sites)

4.3a Seasonal trends

The methods developed and verified at CTR are now applied to the SCAPE study where fewer species were measured. LWC predictions at all SCAPE sites are shown in Table 3, providing insights on seasonal trends of LWC in the southeast. The overall summer LWC mean was 5.0 μg m^{-3} and winter mean 2.2 μg m^{-3}.

At the SCAPE sites, JST, YRK, GIT, and RS, summer mean pHs were between 1 and 1.3, similar to CTR (mean of 0.94). In winter the pHs (mean between 1.8 and 2.2) were higher by ~ 1 unit. Although LWC was higher in summer, which tends to dilute H^+_{air} and increase pH, summer pH was lower due to higher ion (i.e., sulfate) concentrations (Table 3). Similar diurnal pH patterns were seen at all sites in all seasons and follow the diurnal variations of particle water (Figure 11). Overall the pH in the southeast is very low, between 1 and 2 (mean), in both rural and urban environments. pH values in summer at various sites were similar (1 to 1.3), suggesting a fairly homogeneous distribution of acidity due to spatially uniform sulfate in the southeastern US (Zhang et al., 2012). In winter the diurnal range in pH was roughly 2 units, while the diurnal range in summer was smaller, with pH varying by roughly 1.

Recall at CTR, 10% RH uncertainty can result in a pH prediction error of up to 45% due to the high RHs observed during the study. We estimated pH uncertainty from W_i and W_o by + 10% RH for each SCAPE site. As Table 3 shows, the pH uncertainty associated with RH is much lower in winter (only 1-3%) than summer (20-40%), although RH averages were similar, e.g., JST in May (67 ±19%) and Nov (63 ±19%), with even higher RH in winter at YRK. Total pH uncertainty at all SCAPE sites are calculated by the same method as CTR. Table 3 shows that higher RH and T result in larger pH uncertainty. In summer, pH uncertainty is mainly caused by RH; while in winter, it can be attributed mostly to uncertainty in ion concentrations.

4.3b The role of W_o

W_o was significant, accounting for on average 29-39% of the total $PM_{2.5}$ particle water for all our sites (Figure 12 and Table 3). Note that, W_o at SCAPE sites were calculated by in-situ AMS measurements at each SCAPE site and the mean κ_{org} (0.126) measured at CTR, due to lack of CCNc. Note that ε_{W_o} could be higher or lower at each site depending on the type of organics presented and the related κ_{org}. Figure 12 shows that W_o is related to the organic mass fraction. W_o is comparable to W_i at night. In contrast, it was only 33% of W_i during the daytime (Figure 3). The significant fraction, even during daytime,

indicates organic aerosol components will have a considerable contribution to aerosol radiative forcing. Although organics are less hygroscopic than ammonium sulfate, a large fraction of the $PM_{2.5}$ (~70%) was organic, making W_o contributions important. Of the organic factors associated with W_o, Cerully et al. (2014) showed that MO-OOA (more-oxidized oxygenated organic aerosol, also referred to as LVOOA, low-volatile oxygenated organic aerosol) and Isoprene-OA (isoprene derived organic aerosol) were twice as hygroscopic as LO-OOA (less-oxidized oxygenated organic aerosol, also referred to as SVOOA, semi-volatile oxygenated organic aerosol). The LWC associated with MO-OOA and Isoprene-OA account for ~60% and ~30% of total W_o in the daytime, respectively.

The effect of particle water on pH can also be delineated. pH calculated just by W_i alone will be affected by an underestimation of particle water, resulting in a slightly lower pH (Figure 13). W_o is on average 29% to 39% of total water at all sites, as a result pH increases by 0.15 to 0.23 units when W_o is included. Independent of the pH range, a 29% to 39% W_o fraction always increases pH by 0.15 to 0.23 due to the logarithmic nature of pH. The effect of W_o on pH can be simply denoted as $\log_{10}(1 - \varepsilon_{W_o})$. For example, when ε_{W_o} is 90%, it shifts pH up by 1 unit. pH based on W_i is highly correlated with pH for total water ($W_i + W_o$) (Slope = 0.94, intercept = -0.14, R^2 = 0.97). This indicates that if organic mass and κ_{org} are not available, ISORROPIA-II run with only ion data will give a reasonable estimate of pH, since both H^+_{air} and W_i are outputs of ISORROPIA-II, while W_o is predicted based on organic mass and κ_{org}. Accurate temperature and RH are still necessary inputs, especially when RH is high.

4.4 Overall implications of low pH

Highly acidic aerosols throughout the southeast during all seasons will affect a variety of processes. For example, aerosol acidity strongly shifts the partitioning of $HNO_{3(g)}$ to the gas phase resulting in low nitrate aerosol levels in the southeast during summer (the higher summertime temperature also plays a secondary role). Aerosol acidity also impacts the gas-particle partitioning of semi-volatile organic acids. Note, organic acids are not considered in our model, under these acidic conditions (pH = 1) their contributions to the H^+_{air} (hence pH) are expected to be negligible. Because the pK_a (pK_a = - $\log_{10} K_a$, K_a referred as acid dissociation constant) of trace organic acids are > 2 (e.g., pK_a of formic acid, one of the strongest organic acids, is 3.75, Bacarella et al. (1955)), low pH prevents dissociation of the organic acids. Since H^+ is involved in aqueous phase reactions, low pH can affect reaction rates by providing protons. Investigators have found that Isoprene-OA formation is acid-catalyzed and sulfuric acid participates in the reaction as a proton donor in chamber studies (Surratt et al., 2007). However, aerosol acidity appears not to be a limiting factor for Isoprene-OA formation in the southeastern US, owing to the consistently very low pH (Karambelas et al., 2014; Xu et al., 2015). Finally, low pH can affect the solubility of trace metals

(e.g., mineral dust) such as Fe and Cu, which possibly increases the toxicity of the redox metals (Ghio et al., 2012; Verma et al., 2014) and may also have a long term effect on nutrient distributions in the region (Meskhidze et al., 2003; Meskhidze et al., 2005; Nenes et al., 2011; Ito and Xu, 2014).

5 Conclusions

Particle pH is important and difficult to measure directly. However, the commonly used pH proxies of ion balances and NH_4^+/SO_4^{2-} molar ratios do not necessarily correlate with pH. Therefore, predicting pH is the best method to analyze particle acidity. By combining several models we present a comprehensive prediction method to calculate pH and include an uncertainty analysis. ISORROPIA-II is applied to calculate the concentration of H_{air}^+ and W_i from inorganic aerosol measurements, and CCN activity is used to predict W_o. The adjoint model of ISORROPIA, ANISORROPIA, is applied to determine sensitivities, which are used for propagating the measurement uncertainties to pH. We find that W_o should be included when predicting particle LWC when organic loadings are high (such as in the southeastern US). However, the pH prediction is not highly sensitive to W_o, unless W_o mass fraction to the total particle water is close to 1. Thus, in most cases particle pH can be predicted fairly accurately with just measurements of inorganic species and ISORROPIA-II. However, constraining ISORROPIA-II with gas phase species, such as $NH_{3(g)}$, as done in this work (or $HNO_{3(g)}$), is highly recommended, along with running ISORROPIA-II in the forward mode. ISORROPIA-II does not consider organic acids, but at the low pHs of this study, they do not contribute protons (Bacarella et al., 1955). However, when pH approaches 7, the dissociation of organic acids cannot be neglected. Finally, the model was validated through comparing predicted to measured liquid water (W_i+W_o to $f(RH)$_water) and predicted to measured $NH_{3(g)}$ concentrations.

On average, for the SOAS and SCAPE field studies, particle water associated with the $PM_{2.5}$ organic species (W_o) accounted for a significant fraction of total LWC, with a mean of 35% (±3% SD) indicating the importance of organic hygroscopic properties to aqueous phase chemistry and radiative forcing in the southeast US. Although organics are less hygroscopic than sulfate and ammonium, the larger mass fraction of organics than inorganics promotes W_o uptake. Predicted LWC was compared to LWC determined from ambient versus dry light scattering coefficients and a TEOM measurement of dry $PM_{2.5}$ mass. In SOAS, the sum of W_i and W_o was highly correlated and in close agreement with the measured LWC (slope = 0.91, R^2 = 0.75). LWC showed a clear diurnal pattern, with a continuous increase at night (median of 10 μg m^{-3} at 7:30 am) reaching a distinct peak when RH reached a maximum near 90% just after sunrise during the period of lowest daily temperature, followed by a rapid decrease and lower values during the day (median of 2 μg m^{-3} at 2:30 pm).

In the southeastern US, pH normally varied from 0.5 to 2 in the summer and 1 to 3 in the winter, indicating that the aerosol was highly acidic throughout the year. The minimum and maximum pH were -0.94 and 2.2 at CTR, respectively and varied from a nighttime average of 1.5 to daytime average of 0.6, mostly attributable to diurnal variation in RH and temperature. Mean NH_4^+/SO_4^{2-} molar ratios were 1.4 ± 0.5 (SD) and roughly half the ammonia was in the gas phase ($NH_{3(g)}$ / ($NH_{3(g)}$ + NH_4^+) = 41 ± 16 %, mean ± SD). pH at other sites in the southeast (SCAPE study) was estimated based on a limited data set at an estimated uncertainty of 9-49% and a systematic bias of -1 since $NH_{3(g)}$ is not included in the thermodynamic model run in the forward mode. pH can still be predicted with only aerosol measurements, but an adjustment of 1-unit pH increase is recommended for the southeastern US. pH has a diurnal trend that follows LWC, higher (less acidic) at night and lower (more acidic) during the day. pH was also generally higher in the winter (~2) than summer (~1). These low pHs have significant implications for gas-aerosol partitioning, acid-catalyzed reactions including isoprene-OA formation, and trace metal mobilization.

6 Acknowledgements

This work was supported by the NSF under grant number 1242258 as part of the SOAS campaign. GIT SOAS Researchers were also supported by a US EPA STAR grant R835410 and NOAA CPO Award NA10OAR4310102. Measurements at other sites in the southeast were part of the EPA-supported SCAPE Clean Air Center, made possible through US EPA grant R834799. The content of this publication are solely the responsibility of the grantee and do not necessarily represent the official views of the US EPA. Further, US EPA does not endorse the purchase of any commercial products or services mentioned in the publication. SLC was supported by an appointment to the Research Participation Program at the Office of Research and Development, US EPA, administered by ORISE. AN acknowledges support from a Georgia Power Faculty Scholar Chair and a Cullen-Peck Faculty Fellowship from the Georgia Institute of Technology. We also like to thank Dr. Richard Moore from NASA Langley for valuable suggestions and discussions. SHL acknowledges funding support from NSF (AGS-1241498). AB acknowledges support within the framework of the Action Supporting Postdoctoral Researchers of the Operational Program "Education and Lifelong Learning" (Action's Beneficiary: General Secretariat for Research and Technology), and is co-financed by the European Social Fund (ESF) and the Greek State. We wish to thank the Southeastern Aerosol Research and Characterization (SEARCH) personnel for their many contributions supporting the field deployments.

References

Bacarella, A. L., Grunwald, E., Marshall, H. P., and Purlee, E. L.: The Potentiometric Measurement of Acid Dissociation Constants and *p*H in the System Methanol-Water. pK_a Values for Carboxylic Acids and Anilinium Ions, J Org Chem, 20, 747-762, doi: 10.1021/Jo01124a007, 1955.

Bertram, A. K., Martin, S. T., Hanna, S. J., Smith, M. L., Bodsworth, A., Chen, Q., Kuwata, M., Liu, A., You, Y., and Zorn, S. R.: Predicting the relative humidities of liquid-liquid phase separation, efflorescence, and deliquescence of mixed particles of ammonium sulfate, organic material, and water using the organic-to-sulfate mass ratio of the particle and the oxygen-to-carbon elemental ratio of the organic component, Atmospheric Chemistry and Physics, 11, 10995-11006, doi: 10.5194/acp-11-10995-2011, 2011.

Canagaratna, M. R., Jayne, J. T., Jimenez, J. L., Allan, J. D., Alfarra, M. R., Zhang, Q., Onasch, T. B., Drewnick, F., Coe, H., Middlebrook, A., Delia, A., Williams, L. R., Trimborn, A. M., Northway, M. J., DeCarlo, P. F., Kolb, C. E., Davidovits, P., and Worsnop, D. R.: Chemical and microphysical characterization of ambient aerosols with the aerodyne aerosol mass spectrometer, Mass spectrometry reviews, 26, 185-222, doi: 10.1002/mas.20115, 2007.

Capps, S. L., Henze, D. K., Hakami, A., Russell, A. G., and Nenes, A.: ANISORROPIA: the adjoint of the aerosol thermodynamic model ISORROPIA, Atmospheric Chemistry and Physics, 12, 527-543, doi: 10.5194/acp-12-527-2012, 2012.

Carlton, A. G., and Turpin, B. J.: Particle partitioning potential of organic compounds is highest in the Eastern US and driven by anthropogenic water, Atmospheric Chemistry and Physics, 13, 10203-10214, doi: 10.5194/acp-13-10203-2013, 2013.

Carrico, C. M., Rood, M. J., and Ogren, J. A.: Aerosol light scattering properties at Cape Grim, Tasmania, during the First Aerosol Characterization Experiment (ACE 1), Journal of Geophysical Research, 103, 16565, doi: 10.1029/98jd00685, 1998.

Carrico, C. M., Rood, M. J., Ogren, J. A., Neususs, C., Wiedensohler, A., and Heintzenberg, J.: Aerosol optical properties at Sagres, Portugal during ACE-2, Tellus B, 52, 694-715, doi: 10.1034/j.1600-0889.2000.00049.x, 2000.

Cerully, K. M., Bougiatioti, A., Hite Jr, J. R., Guo, H., Xu, L., Ng, N. L., Weber, R., and Nenes, A.: On the link between hygroscopicity, volatility, and oxidation state of ambient and water-soluble aerosol in the Southeastern United States, Atmospheric Chemistry and Physics Discussions, 14, 30835-30877, doi: 10.5194/acpd-14-30835-2014, 2014.

Clegg, S. L., Brimblecombe, P., and Wexler, A. S.: Thermodynamic model of the system H^+-NH_4^+-SO_4^{2-}-NO_3^--H_2O at tropospheric temperatures, J Phys Chem A, 102, 2137-2154, doi: 10.1021/Jp973042r, 1998.

Czoschke, N. M., and Jang, M.: Acidity effects on the formation of α-pinene ozone SOA in the presence of inorganic seed, Atmospheric Environment, 40, 4370-4380, doi: 10.1016/j.atmosenv.2006.03.030, 2006.

DeCarlo, P. F., Kimmel, J. R., Trimborn, A., Northway, M. J., Jayne, J. T., Aiken, A. C., Gonin, M., Fuhrer, K., Horvath, T., Docherty, K. S., Worsnop, D. R., and Jimenez, J. L.: Field-deployable, high-resolution, time-of-flight aerosol mass spectrometer, Analytical chemistry, 78, 8281-8289, doi: 10.1021/ac061249n, 2006.

Eddingsaas, N. C., VanderVelde, D. G., and Wennberg, P. O.: Kinetics and Products of the Acid-Catalyzed Ring-Opening of Atmospherically Relevant Butyl Epoxy Alcohols, J Phys Chem A, 114, 8106-8113, doi: 10.1021/Jp103907c, 2010.

Edney, E. O., Kleindienst, T. E., Jaoui, M., Lewandowski, M., Offenberg, J. H., Wang, W., and Claeys, M.: Formation of 2-methyl tetrols and 2-methylglyceric acid in secondary organic aerosol from laboratory irradiated isoprene/NO_X/SO_2/air mixtures and their detection in ambient $PM_{2.5}$ samples collected in the eastern United States, Atmospheric Environment, 39, 5281-5289, doi: 10.1016/j.atmosenv.2005.05.031, 2005.

Engelhart, G. J., Asa-Awuku, A., Nenes, A., and Pandis, S. N.: CCN activity and droplet growth kinetics of fresh and aged monoterpene secondary organic aerosol, Atmospheric Chemistry and Physics, 8, 3937-3949, doi: 10.5194/acp-8-3937-2008, 2008.

Ervens, B., Turpin, B. J., and Weber, R. J.: Secondary organic aerosol formation in cloud droplets and aqueous particles (aqSOA): a review of laboratory, field and model studies, Atmospheric Chemistry and Physics Discussions, 11, 22301-22383, doi: 10.5194/acpd-11-22301-2011, 2011.

Fountoukis, C., and Nenes, A.: ISORROPIA II: a computationally efficient thermodynamic equilibrium model for K^+-Ca^{2+}-Mg^{2+}-NH_4^+-Na^+-SO_4^{2-}-NO_3^--Cl^--H_2O aerosols, Atmospheric Chemistry and Physics, 7, 4639-4659, doi: 10.5194/acp-7-4639-2007, 2007.

Fountoukis, C., Nenes, A., Sullivan, A., Weber, R., Van Reken, T., Fischer, M., Matias, E., Moya, M., Farmer, D., and Cohen, R. C.: Thermodynamic characterization of Mexico City aerosol during MILAGRO 2006, Atmospheric Chemistry and Physics, 9, 2141-2156, doi: 10.5194/acp-9-2141-2009, 2009.

Frosch, M., Bilde, M., DeCarlo, P. F., Jurányi, Z., Tritscher, T., Dommen, J., Donahue, N. M., Gysel, M., Weingartner, E., and Baltensperger, U.: Relating cloud condensation nuclei activity and oxidation level of α-pinene secondary organic aerosols, Journal of Geophysical Research: Atmospheres, 116, doi: 10.1029/2011jd016401, 2011.

Gao, S., Keywood, M., Ng, N. L., Surratt, J., Varutbangkul, V., Bahreini, R., Flagan, R. C., and Seinfeld, J. H.: Low-molecular-weight and oligomeric components in secondary organic aerosol from the ozonolysis of cycloalkenes and alpha-pinene, J Phys Chem A, 108, 10147-10164, doi: 10.1021/Jp047466e, 2004.

Ghio, A. J., Carraway, M. S., and Madden, M. C.: Composition of air pollution particles and oxidative stress in cells, tissues, and living systems, Journal of toxicology and environmental health. Part B, Critical reviews, 15, 1-21, doi: 10.1080/10937404.2012.632359, 2012.

Hansen, D. A., Edgerton, E. S., Hartsell, B. E., Jansen, J. J., Kandasamy, N., Hidy, G. M., and Blanchard, C. L.: The Southeastern Aerosol Research and Characterization Study: Part 1—Overview, Journal of the Air & Waste Management Association, 53, 1460-1471, doi: 10.1080/10473289.2003.10466318, 2003.

Hansen, D. A., Edgerton, E., Hartsell, B., Jansen, J., Burge, H., Koutrakis, P., Rogers, C., Suh, H., Chow, J., Zielinska, B., McMurry, P., Mulholland, J., Russell, A., and Rasmussen, R.: Air Quality Measurements for the Aerosol Research and Inhalation Epidemiology Study, Journal of the Air & Waste Management Association, 56, 1445-1458, doi: 10.1080/10473289.2006.10464549, 2006.

Hennigan, C. J., Bergin, M. H., Dibb, J. E., and Weber, R. J.: Enhanced secondary organic aerosol formation due to water uptake by fine particles, Geophysical Research Letters, 35, L18801, doi: 10.1029/2008gl035046, 2008.

Hennigan, C. J., Izumi, J., Sullivan, A. P., Weber, R. J., and Nenes, A.: A critical evaluation of proxy methods used to estimate the acidity of atmospheric particles, Atmospheric Chemistry and Physics Discussions, 14, 27579-27618, doi: 10.5194/acpd-14-27579-2014, 2014.

Hildebrandt Ruiz, L., Paciga, A. L., Cerully, K., Nenes, A., Donahue, N. M., and Pandis, S. N.: Aging of secondary organic aerosol from small aromatic VOCs: changes in chemical composition, mass yield, volatility and hygroscopicity, Atmospheric Chemistry and Physics Discussions, 14, 31441-31481, doi: 10.5194/acpd-14-31441-2014, 2014.

Iinuma, Y., Böge, O., Gnauk, T., and Herrmann, H.: Aerosol-chamber study of the α-pinene/O_3 reaction: influence of particle acidity on aerosol yields and products, Atmospheric Environment, 38, 761-773, doi: 10.1016/j.atmosenv.2003.10.015, 2004.

IPCC: Climate Change 2013: The Physical Science Basis. Contribution of Working Group I to the Fifth Assessment Report of the Intergovernmental Panel on Climate Change, Cambridge University Press, Cambridge, United Kingdom and New York, NY, USA, 1535 pp., 2013.

Ito, A., and Xu, L.: Response of acid mobilization of iron-containing mineral dust to improvement of air quality projected in the future, Atmospheric Chemistry and Physics, 14, 3441-3459, doi: 10.5194/acp-14-3441-2014, 2014.

713 Jang, M., Czoschke, N. M., Lee, S., and Kamens, R. M.: Heterogeneous atmospheric aerosol production
714 by acid-catalyzed particle-phase reactions, Science, 298, 814-817, doi: 10.1126/science.1075798,
715 2002.
716 Karambelas, A., Pye, H. O. T., Budisulistiorini, S. H., Surratt, J. D., and Pinder, R. W.: Contribution of
717 Isoprene Epoxydiol to Urban Organic Aerosol: Evidence from Modeling and Measurements,
718 Environmental Science & Technology Letters, 1, 278-283, doi: 10.1021/ez5001353, 2014.
719 Kim, J., Yoon, S.-C., Jefferson, A., and Kim, S.-W.: Aerosol hygroscopic properties during Asian dust,
720 pollution, and biomass burning episodes at Gosan, Korea in April 2001, Atmospheric
721 Environment, 40, 1550-1560, doi: 10.1016/j.atmosenv.2005.10.044, 2006.
722 King, S. M., Rosenoern, T., Shilling, J. E., Chen, Q., and Martin, S. T.: Cloud condensation nucleus
723 activity of secondary organic aerosol particles mixed with sulfate, Geophysical Research Letters,
724 34, L24806, doi: 10.1029/2007gl030390, 2007.
725 Kleindienst, T. E., Edney, E. O., Lewandowski, M., Offenberg, J. H., and Jaoui, M.: Secondary organic
726 carbon and aerosol yields from the irradiations of isoprene and α-pinene in the presence of NO_x
727 and SO_2, Environmental science & technology, 40, 3807-3812, doi: 10.1021/Es052446r, 2006.
728 Kotchenruther, R. A., and Hobbs, P. V.: Humidification factors of aerosols from biomass burning in
729 Brazil, Journal of Geophysical Research, 103, 32081, doi: 10.1029/98jd00340, 1998.
730 Kuwata, M., Zorn, S. R., and Martin, S. T.: Using elemental ratios to predict the density of organic
731 material composed of carbon, hydrogen, and oxygen, Environmental science & technology, 46,
732 787-794, doi: 10.1021/es202525q, 2012.
733 Lance, S., Nenes, A., Medina, J., and Smith, J. N.: Mapping the Operation of the DMT Continuous Flow
734 CCN Counter, Aerosol Science and Technology, 40, 242-254, doi: 10.1080/02786820500543290,
735 2006.
736 Liao, H., and Seinfeld, J. H.: Global impacts of gas-phase chemistry-aerosol interactions on direct
737 radiative forcing by anthropogenic aerosols and ozone, J Geophys Res-Atmos, 110, D18208, doi:
738 10.1029/2005jd005907, 2005.
739 Liu, J., Zhang, X., Parker, E. T., Veres, P. R., Roberts, J. M., de Gouw, J. A., Hayes, P. L., Jimenez, J. L.,
740 Murphy, J. G., Ellis, R. A., Huey, L. G., and Weber, R. J.: On the gas-particle partitioning of
741 soluble organic aerosol in two urban atmospheres with contrasting emissions: 2. Gas and particle
742 phase formic acid, Journal of Geophysical Research, 117, D00V21, doi: 10.1029/2012jd017912,
743 2012.
744 Magi, B. I., and Hobbs, P. V.: Effects of humidity on aerosols in southern Africa during the biomass
745 burning season, Journal of Geophysical Research, 108, 8495, doi: 10.1029/2002jd002144, 2003.
746 Malm, W. C., and Day, D. E.: Estimates of aerosol species scattering characteristics as a function of
747 relative humidity, Atmospheric Environment, 35, 2845-2860, doi: 10.1016/S1352-
748 2310(01)00077-2, 2001.
749 Meskhidze, N., Chameides, W. L., Nenes, A., and Chen, G.: Iron mobilization in mineral dust: Can
750 anthropogenic SO_2 emissions affect ocean productivity?, Geophysical Research Letters, 30, 2085,
751 doi: 10.1029/2003gl018035, 2003.
752 Meskhidze, N., Chameides, W. L., and Nenes, A.: Dust and pollution: A recipe for enhanced ocean
753 fertilization?, Journal of Geophysical Research, 110, D03301, doi: 10.1029/2004jd005082, 2005.
754 Mitchell, R. M., Campbell, S. K., Qin, Y., and Gras, J. L.: Performance Characteristics of Integrating
755 Nephelometers in the Australian Outback, Journal of Atmospheric and Oceanic Technology, 26,
756 984-995, doi: 10.1175/2008jtecha1187.1, 2009.
757 Nemesure, S., Wagener, R., and Schwartz, S. E.: Direct shortwave forcing of climate by the
758 anthropogenic sulfate aerosol: Sensitivity to particle size, composition, and relative humidity, J
759 Geophys Res-Atmos, 100, 26105-26116, doi: 10.1029/95jd02897, 1995.
760 Nenes, A., Pandis, S. N., and Pilinis, C.: ISORROPIA: A new thermodynamic equilibrium model for
761 multiphase multicomponent inorganic aerosols, Aquat Geochem, 4, 123-152, doi:
762 10.1023/A:1009604003981, 1998.

763 Nenes, A., Krom, M. D., Mihalopoulos, N., Van Cappellen, P., Shi, Z., Bougiatioti, A., Zarmpas, P., and
764 Herut, B.: Atmospheric acidification of mineral aerosols: a source of bioavailable phosphorus for
765 the oceans, Atmospheric Chemistry and Physics, 11, 6265-6272, doi: 10.5194/acp-11-6265-2011,
766 2011.
767 Nguyen, T. B., Coggon, M. M., Flagan, R. C., and Seinfeld, J. H.: Reactive uptake and photo-Fenton
768 oxidation of glycolaldehyde in aerosol liquid water, Environmental science & technology, 47,
769 4307-4316, doi: 10.1021/es400538j, 2013.
770 Nguyen, T. K. V., Petters, M. D., Suda, S. R., Guo, H., Weber, R. J., and Carlton, A. G.: Trends in
771 particle-phase liquid water during the Southern Oxidant and Aerosol Study, Atmospheric
772 Chemistry and Physics, 14, 10911-10930, doi: 10.5194/acp-14-10911-2014, 2014.
773 Nowak, J. B., Huey, L. G., Russell, A. G., Tian, D., Neuman, J. A., Orsini, D., Sjostedt, S. J., Sullivan, A.
774 P., Tanner, D. J., Weber, R. J., Nenes, A., Edgerton, E., and Fehsenfeld, F. C.: Analysis of urban
775 gas phase ammonia measurements from the 2002 Atlanta Aerosol Nucleation and Real-Time
776 Characterization Experiment (ANARChE), Journal of Geophysical Research, 111, D17308, doi:
777 10.1029/2006jd007113, 2006.
778 Orsini, D. A., Ma, Y., Sullivan, A., Sierau, B., Baumann, K., and Weber, R. J.: Refinements to the
779 particle-into-liquid sampler (PILS) for ground and airborne measurements of water soluble
780 aerosol composition, Atmospheric Environment, 37, 1243-1259, doi: 10.1016/s1352-
781 2310(02)01015-4, 2003.
782 Pathak, R. K., Wang, T., Ho, K. F., and Lee, S. C.: Characteristics of summertime $PM_{2.5}$ organic and
783 elemental carbon in four major Chinese cities: Implications of high acidity for water-soluble
784 organic carbon (WSOC), Atmospheric Environment, 45, 318-325, doi:
785 10.1016/j.atmosenv.2010.10.021, 2011.
786 Petters, M. D., and Kreidenweis, S. M.: A single parameter representation of hygroscopic growth and
787 cloud condensation nucleus activity, Atmospheric Chemistry and Physics, 7, 1961-1971, 2007.
788 Pilinis, C., Pandis, S. N., and Seinfeld, J. H.: Sensitivity of Direct Climate Forcing by Atmospheric
789 Aerosols to Aerosol-Size and Composition, J Geophys Res-Atmos, 100, 18739-18754, doi:
790 10.1029/95jd02119, 1995.
791 Pye, H. O., Pinder, R. W., Piletic, I. R., Xie, Y., Capps, S. L., Lin, Y. H., Surratt, J. D., Zhang, Z., Gold,
792 A., Luecken, D. J., Hutzell, W. T., Jaoui, M., Offenberg, J. H., Kleindienst, T. E., Lewandowski,
793 M., and Edney, E. O.: Epoxide pathways improve model predictions of isoprene markers and
794 reveal key role of acidity in aerosol formation, Environmental science & technology, 47, 11056-
795 11064, doi: 10.1021/es402106h, 2013.
796 Roberts, G. C., and Nenes, A.: A Continuous-Flow Streamwise Thermal-Gradient CCN Chamber for
797 Atmospheric Measurements, Aerosol Science and Technology, 39, 206-221, doi:
798 10.1080/027868290913988, 2005.
799 Seinfeld, J. H., and Pandis, S. N.: Atmospheric Chemistry and Physics: from Air Pollution to Climate
800 Change 2nd Edition, John Wiley & Sons, Inc., Hoboken, New Jersey, 2006.
801 Sheridan, P. J., Jefferson, A., and Ogren, J. A.: Spatial variability of submicrometer aerosol radiative
802 properties over the Indian Ocean during INDOEX, Journal of Geophysical Research, 107, 8011,
803 doi: 10.1029/2000jd000166, 2002.
804 Sloane, C. S., Watson, J., Chow, J., Pritchett, L., and Richards, L. W.: Size-Segregated Fine Particle
805 Measurements by Chemical-Species and Their Impact on Visibility Impairment in Denver,
806 Atmospheric Environment. Part A. General Topics, 25, 1013-1024, doi: 10.1016/0960-
807 1686(91)90143-U, 1991.
808 Song, M., Marcolli, C., Krieger, U. K., Zuend, A., and Peter, T.: Liquid-liquid phase separation and
809 morphology of internally mixed dicarboxylic acids/ammonium sulfate/water particles,
810 Atmospheric Chemistry and Physics, 12, 2691-2712, doi: 10.5194/acp-12-2691-2012, 2012.
811 Song, M., Liu, P. F., Hanna, S. J., Martin, S. T., and Bertram, A. K.: Relative humidity-dependent
812 viscosities of isoprene-derived secondary organic material and atmospheric implications for

isoprene-dominant forests, Atmos. Chem. Phys. Discuss., 15, 1131-1169, doi: 10.5194/acpd-15-1131-2015, 2015.

Sorooshian, A., Hersey, S., Brechtel, F. J., Corless, A., Flagan, R. C., and Seinfeld, J. H.: Rapid, Size-Resolved Aerosol Hygroscopic Growth Measurements: Differential Aerosol Sizing and Hygroscopicity Spectrometer Probe (DASH-SP), Aerosol Science and Technology, 42, 445-464, doi: 10.1080/02786820802178506, 2008.

Stein, S. W., Turpin, B. J., Cai, X. P., Huang, C. P. F., and Mcmurry, P. H.: Measurements of Relative Humidity-Dependent Bounce and Density for Atmospheric Particles Using the DMA-Impactor Technique, Atmospheric Environment, 28, 1739-1746, doi: 10.1016/1352-2310(94)90136-8, 1994.

Stokes, R. H., and Robinson, R. A.: Interactions in Aqueous Nonelectrolyte Solutions .I. Solute-Solvent Equilibria, Journal of Physical Chemistry, 70, 2126-2130, doi: Doi 10.1021/J100879a010, 1966.

Surratt, J. D., Lewandowski, M., Offenberg, J. H., Jaoui, M., Kleindienst, T. E., Edney, E. O., and Seinfeld, J. H.: Effect of acidity on secondary organic aerosol formation from isoprene, Environmental science & technology, 41, 5363-5369, doi: 10.1021/es0704176, 2007.

Surratt, J. D., Chan, A. W., Eddingsaas, N. C., Chan, M., Loza, C. L., Kwan, A. J., Hersey, S. P., Flagan, R. C., Wennberg, P. O., and Seinfeld, J. H.: Reactive intermediates revealed in secondary organic aerosol formation from isoprene, Proceedings of the National Academy of Sciences of the United States of America, 107, 6640-6645, doi: 10.1073/pnas.0911114107, 2010.

Tang, I. N.: Phase transformation and growth of aerosol particles composed of mixed salts, Journal of Aerosol Science, 7, 361-371, doi: 10.1016/0021-8502(76)90022-7, 1976.

Tang, I. N., and Munkelwitz, H. R.: Composition and Temperature-Dependence of the Deliquescence Properties of Hygroscopic Aerosols, Atmospheric Environment. Part A. General Topics, 27, 467-473, doi: Doi 10.1016/0960-1686(93)90204-C, 1993.

Tanner, R. L., Olszyna, K. J., Edgerton, E. S., Knipping, E., and Shaw, S. L.: Searching for evidence of acid-catalyzed enhancement of secondary organic aerosol formation using ambient aerosol data, Atmospheric Environment, 43, 3440-3444, doi: 10.1016/j.atmosenv.2009.03.045, 2009.

Tolocka, M. P., Jang, M., Ginter, J. M., Cox, F. J., Kamens, R. M., and Johnston, M. V.: Formation of oligomers in secondary organic aerosol, Environmental science & technology, 38, 1428-1434, doi: 10.1021/es035030r, 2004.

Turpin, B. J., and Lim, H.-J.: Species Contributions to PM2.5 Mass Concentrations: Revisiting Common Assumptions for Estimating Organic Mass, Aerosol Science and Technology, 35, 602-610, doi: 10.1080/02786820119445, 2001.

Verma, V., Fang, T., Guo, H., King, L., Bates, J. T., Peltier, R. E., Edgerton, E., Russell, A. G., and Weber, R. J.: Reactive oxygen species associated with water-soluble $PM_{2.5}$ in the southeastern United States: spatiotemporal trends and source apportionment, Atmospheric Chemistry and Physics, 14, 12915-12930, doi: 10.5194/acp-14-12915-2014, 2014.

Villani, P., Sellegri, K., Monier, M., and Laj, P.: Influence of semi-volatile species on particle hygroscopic growth, Atmospheric Environment, 79, 129-137, doi: 10.1016/j.atmosenv.2013.05.069, 2013.

Wexler, A. S., and Seinfeld, J. H.: Second-generation inorganic aerosol model, Atmospheric Environment. Part A. General Topics, 25, 2731-2748, doi: 10.1016/0960-1686(91)90203-J, 1991.

Xu, L., Guo, H., Boyd, C. M., Klein, M., Bougiatioti, A., Cerully, K. M., Hite, J. R., Isaacman-VanWertz, G., Kreisberg, N. M., Knote, C., Olson, K., Koss, A., Goldstein, A. H., Hering, S. V., de Gouw, J., Baumann, K., Lee, S.-H., Nenes, A., Weber, R. J., and Ng, N. L.: Effects of anthropogenic emissions on aerosol formation from isoprene and monoterpenes in the southeastern United States, Proceedings of the National Academy of Sciences, 112, 37-42, doi: 10.1073/pnas.1417609112, 2015.

Yin, L., Niu, Z., Chen, X., Chen, J., Zhang, F., and Xu, L.: Characteristics of water-soluble inorganic ions in $PM_{2.5}$ and $PM_{2.5-10}$ in the coastal urban agglomeration along the Western Taiwan Strait Region,

863 China, Environmental science and pollution research international, 21, 5141-5156, doi:
864 10.1007/s11356-013-2134-7, 2014.
865 You, Y., Renbaum-Wolff, L., Carreras-Sospedra, M., Hanna, S. J., Hiranuma, N., Kamal, S., Smith, M. L.,
866 Zhang, X., Weber, R. J., Shilling, J. E., Dabdub, D., Martin, S. T., and Bertram, A. K.: Images
867 reveal that atmospheric particles can undergo liquid-liquid phase separations, Proceedings of the
868 National Academy of Sciences of the United States of America, 109, 13188-13193, doi:
869 10.1073/pnas.1206414109, 2012.
870 You, Y., Renbaum-Wolff, L., and Bertram, A. K.: Liquid–liquid phase separation in particles containing
871 organics mixed with ammonium sulfate, ammonium bisulfate, ammonium nitrate or sodium
872 chloride, Atmospheric Chemistry and Physics, 13, 11723-11734, doi: 10.5194/acp-13-11723-
873 2013, 2013.
874 You, Y., Kanawade, V. P., de Gouw, J. A., Guenther, A. B., Madronich, S., Sierra-Hernandez, M. R.,
875 Lawler, M., Smith, J. N., Takahama, S., Ruggeri, G., Koss, A., Olson, K., Baumann, K., Weber,
876 R. J., Nenes, A., Guo, H., Edgerton, E. S., Porcelli, L., Brune, W. H., Goldstein, A. H., and Lee, S.
877 H.: Atmospheric amines and ammonia measured with a chemical ionization mass spectrometer
878 (CIMS), Atmospheric Chemistry and Physics, 14, 12181-12194, doi: 10.5194/acp-14-12181-2014,
879 2014.
880 Zdanovskii, A. B.: Trudy Solyanoi Laboratorii Akad, Nauk SSSR, 2, 1936.
881 Zhang, X., Liu, Z., Hecobian, A., Zheng, M., Frank, N. H., Edgerton, E. S., and Weber, R. J.: Spatial and
882 seasonal variations of fine particle water-soluble organic carbon (WSOC) over the southeastern
883 United States: implications for secondary organic aerosol formation, Atmospheric Chemistry and
884 Physics, 12, 6593-6607, doi: 10.5194/acp-12-6593-2012, 2012.
885 Zuend, A., Marcolli, C., Peter, T., and Seinfeld, J. H.: Computation of liquid-liquid equilibria and phase
886 stabilities: implications for RH-dependent gas/particle partitioning of organic-inorganic aerosols,
887 Atmospheric Chemistry and Physics, 10, 7795-7820, doi: 10.5194/acp-10-7795-2010, 2010.
888 Zuend, A., and Seinfeld, J. H.: Modeling the gas-particle partitioning of secondary organic aerosol: the
889 importance of liquid-liquid phase separation, Atmospheric Chemistry and Physics, 12, 3857-3882,
890 doi: 10.5194/acp-12-3857-2012, 2012.

891

892

893

894 **Table. 1.** Deployment status of instruments at various sites. All the listed instruments or probes were
895 operated at CTR for SOAS.

Site	Period (mm yyyy)	PILS-IC	AMS	CCNc	Nephelometer	TEOM	RH&T
JST	May&Nov 2012	NO	YES	NO	NO	YES	YES
YRK	Jul&Dec 2012	NO	YES	NO	NO	YES	YES
GIT	Jul-Aug 2012	NO	YES	NO	NO	YES	YES
RS	Sept 2012	NO	YES	NO	NO	YES	YES
CTR	Jun-Jul 2013	YES	YES	YES	YES	YES	YES

896

Table. 2. Sensitivity of H^+_{air} to ions from ANISORROPIA (2nd row) and contribution to uncertainty. Uncertainties of inorganic ions ($\frac{\delta_{Ion}}{Ion}$) are calculated based on a combination of PILS-IC instrumental relative uncertainties (IC uncertainty, referred to as $\frac{\delta_{ion,IC}}{Ion}$, all estimated to be 15%) and the difference between PILS-IC and AMS ($\frac{\delta_{Ion,IC-AMS}}{Ion}$, defined as the (slope – 1) in Figure 2a & 2b) (3rd row), where $\frac{\delta_{Ion}}{Ion} = \sqrt{\left(\frac{\delta_{ion,IC}}{Ion}\right)^2 + \left(\frac{\delta_{Ion,IC-AMS}}{Ion}\right)^2}$ (4th row). Contribution of uncertainty is the ratio of ion uncertainty over H^+_{air} uncertainty ($\frac{\delta_{H^+_{air}}}{H^+_{air}}$, calculated to be 14% in Equation 8) (5th row).

PILS-IC ion concentration, μg m^{-3} (mean ± SD)	SO_4	NH_4^+	Na^+	NO_3^-	Cl^-
	1.73 ± 1.21	0.46 ± 0.34	0.03 ± 0.07	0.08 ± 0.08	0.02 ± 0.03
H^+_{air} Sensitivity (mean ± SD)	$\left\|\frac{\partial H^+_{air}}{\partial SO_4}\right\|$	$\left\|\frac{\partial H^+_{air}}{\partial NH_4^+}\right\|$	$\left\|\frac{\partial H^+_{air}}{\partial Na^+}\right\|$	$\left\|\frac{\partial H^+_{air}}{\partial NO_3^-}\right\|$	$\left\|\frac{\partial H^+_{air}}{\partial Cl^-}\right\|$
	0.51 ± 0.34	0.32 ± 0.31	0.19 ± 0.27	0.002 ± 0.007	0.000 ± 0
$\frac{\delta_{Ion,IC-AMS}}{Ion}$	$\frac{\delta_{SO_4,IC-AMS}}{SO_4}$	$\frac{\delta_{NH_4^+,IC-AMS}}{NH_4^+}$	$\frac{\delta_{Na^+,IC-AMS}}{Na^+}$	$\frac{\delta_{NO_3^-,IC-AMS}}{NO_3^-}$	$\frac{\delta_{Cl^-,IC-AMS}}{Cl^-}$
	20.5%	1.5%	N/A*	**	**
$\frac{\delta_{Ion}}{Ion}$	$\frac{\delta_{SO_4}}{SO_4}$	$\frac{\delta_{NH_4^+}}{NH_4^+}$	$\frac{\delta_{Na^+}}{Na^+}$	$\frac{\delta_{NO_3^-}}{NO_3^-}$	$\frac{\delta_{Cl^-}}{Cl^-}$
	25.4%	15.1%	15%	15%	15%
Contribution to H^+_{air} uncertainty	$\frac{\left\|\frac{\partial H^+_{air}}{\partial SO_4}\right\| \cdot \frac{\delta_{SO_4}}{SO_4}}{\frac{\delta_{H^+_{air}}}{H^+_{air}}}$	$\frac{\left\|\frac{\partial H^+_{air}}{\partial NH_4^+}\right\| \cdot \frac{\delta_{NH_4^+}}{NH_4^+}}{\frac{\delta_{H^+_{air}}}{H^+_{air}}}$	$\frac{\left\|\frac{\partial H^+_{air}}{\partial Na^+}\right\| \cdot \frac{\delta_{Na^+}}{Na^+}}{\frac{\delta_{H^+_{air}}}{H^+_{air}}}$	$\frac{\left\|\frac{\partial H^+_{air}}{\partial NO_3^-}\right\| \cdot \frac{\delta_{NO_3^-}}{NO_3^-}}{\frac{\delta_{H^+_{air}}}{H^+_{air}}}$	$\frac{\left\|\frac{\partial H^+_{air}}{\partial Cl^-}\right\| \cdot \frac{\delta_{Cl^-}}{Cl^-}}{\frac{\delta_{H^+_{air}}}{H^+_{air}}}$
	0.93	0.35	0.20	0.002	0.000

* Na^+ is not measured by AMS.

** $\left|\frac{\partial H^+_{air}}{\partial NO_3^-}\right|$ and $\left|\frac{\partial H^+_{air}}{\partial Cl^-}\right|$ are less than 1% of the other H^+_{air} sensitivities, and the loadings of NO_3^- and Cl^- are less than 5% of the total inorganic ion mass. As a result, their contributions to H^+_{air} uncertainty are negligible.

908 **Table. 3.** Water and pH prediction for SCAPE sites. Means and SDs are listed, if not specified. Total ion
909 concentration is counted as the sum of AMS inorganics (3rd row). ε_{W_o} is the mass fraction of W_o (5th row).

	JST 05/2012	YRK 07/2012	GIT 08/2012	RS 09/2012	JST 11/2012	YRK 12/2012
RH, %	67 ±19	66 ±21	71 ±17	72 ±20	63 ±19	73 ±21
T, ℃	23 ±4	28 ±4	26 ±4	21 ±4	12 ±5	10 ±5
Total ion concentration, μg m^{-3}	4.1 ±2.1	4.5 ±2.2	5.3 ±2.6	4.1 ±2.7	3.6 ±2.1	2.3 ±1.8
$\frac{\delta_{pH}}{pH}$ from 1.10RH	22.3%	21.4%	48.3%	22.1%	2.5%	1.4%
Total $\frac{\delta_{pH}}{pH}$	23.9%	23.0%	49.0%	23.7%	8.8%	8.6%
ε_{W_o}, %	34 ±11	37 ±8	33 ±10	38 ±11	39 ±16	29 ±15
LWC, μg m^{-3}	6.0 ±6.3	8.1 ±8.5	8.4 ±7.7	7.8 ±9.2	5.9 ±8.7	3.2 ±3.5
pH*	1.3 ±0.7	1.1 ±0.6	1.1 ±0.4	1.3 ±0.7	2.2 ±0.9	1.8 ±1.0
LWC, μg m^{-3} (median)	3.7 ±6.3	5.3 ±8.5	6.1 ±7.7	4.3 ±9.2	2.1 ±8.7	2.0 ±3.5
pH* (median)	1.2 ±0.7	1.0 ±0.6	1.0 ±0.4	1.2 ±0.7	2.3 ±0.9	1.8 ±1.0

910 * A bias correction of 1 pH unit is applied due to not considering ammonia partitioning. See Section 4.2c
911 for details.

912

913

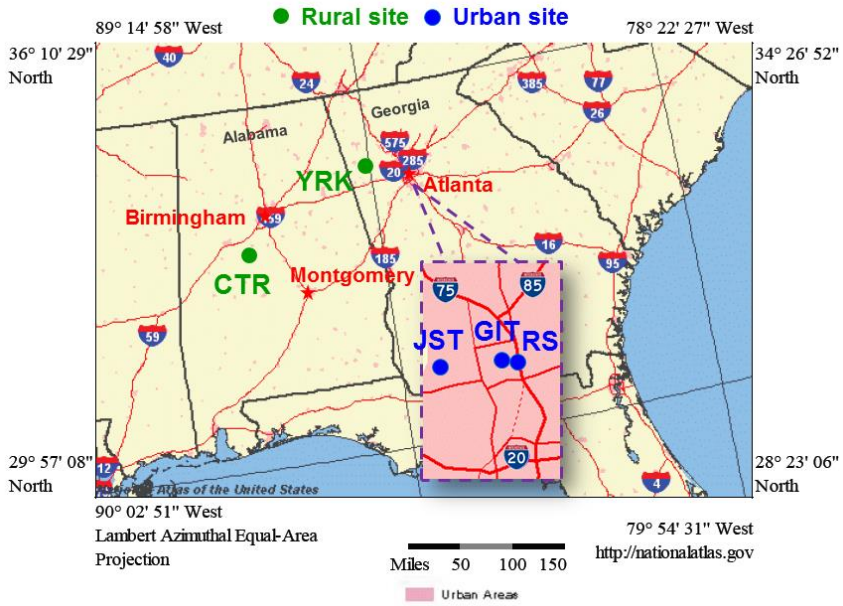

914

915 **Fig. 1.** Sampling sites in the southeastern US, consisting of two rural and three urban sites.

916

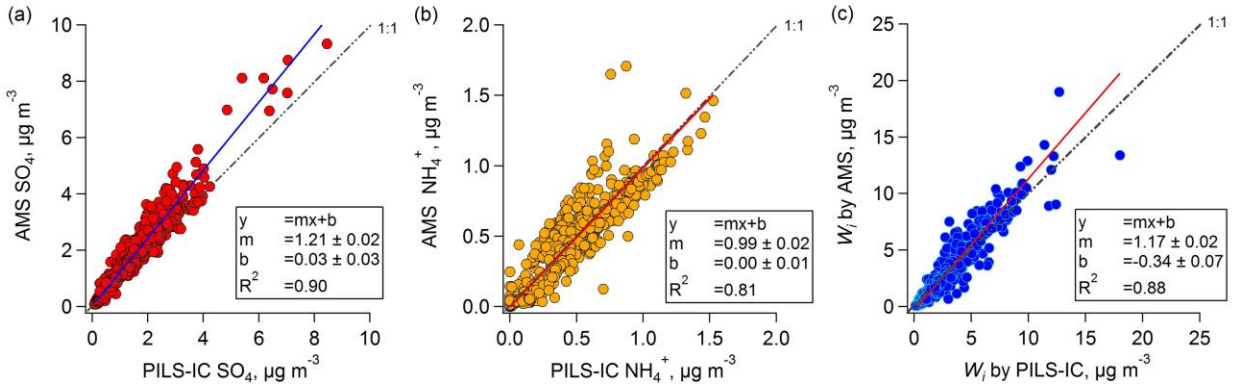

Fig. 2. Comparisons of PM_1 AMS sulfate, ammonium to PM_1 and $PM_{2.5}$ PILS-IC (i.e. complete SOAS study) and predicted W_i. Orthogonal distance regression (ODR) fits were applied.

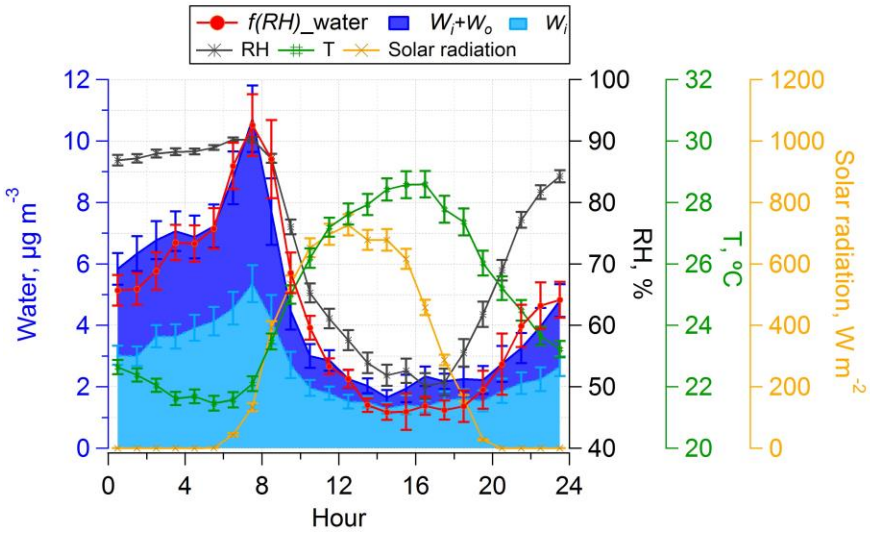

Fig. 3. CTR (SOAS) diurnal profiles of predicted and measured water, measured RH, T, and solar radiation. Median hourly averages are shown and standard errors are plotted as error bars.

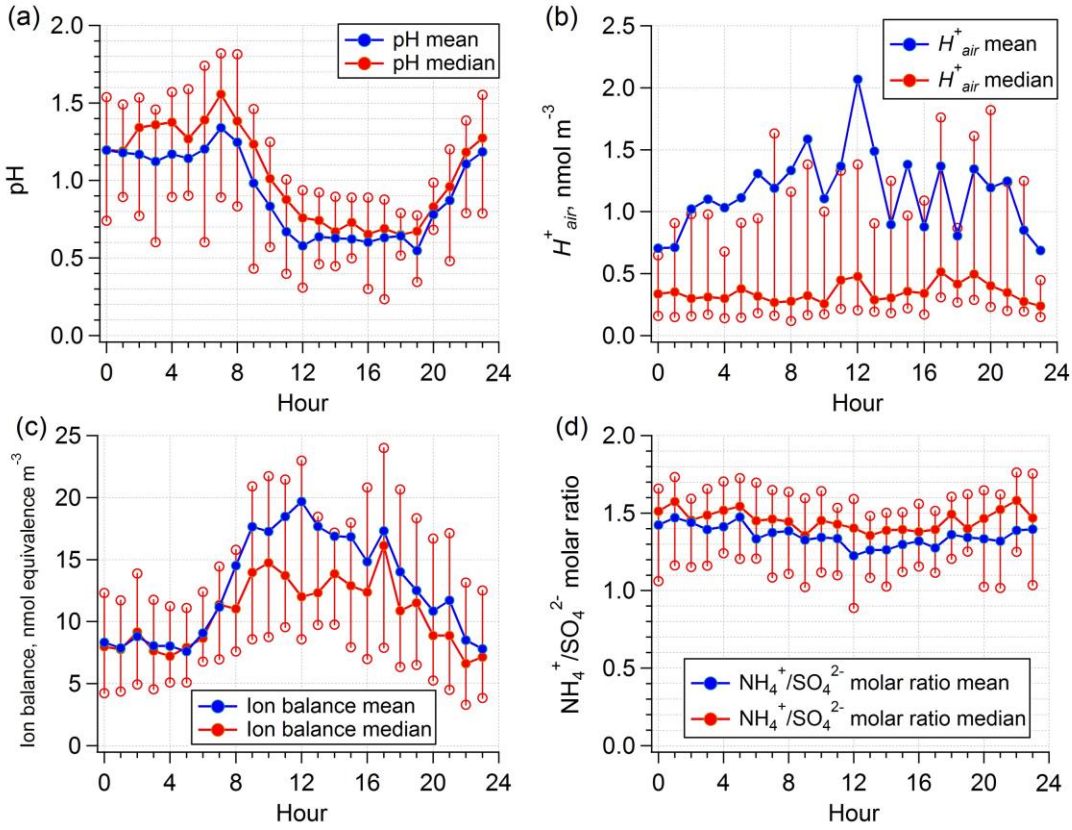

Fig. 4. CTR (SOAS) diurnal patterns of calculated pH based on total predicted water (W_i + W_o) (a), H^+_{air} predicted by ISORROPIA-II (b), ion balance (c), and NH_4^+/SO_4^{2-} molar ratio (d). Mean and median values are shown, together with 25% and 75% quantiles marked as non-filled circles.

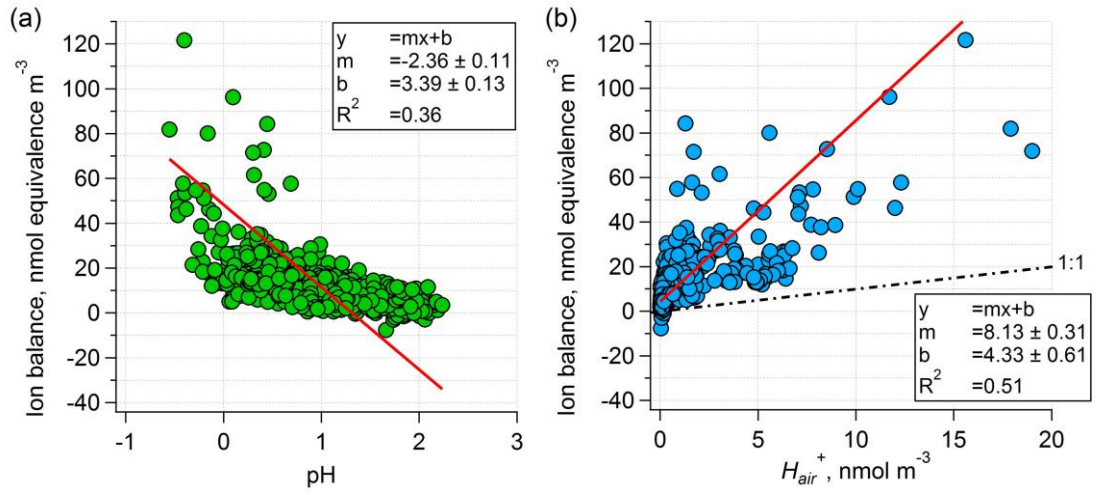

Fig. 5. Comparison of ion balance to pH (a) and to H^+_{air} (b) at CTR (SOAS). An ODR fit was applied.

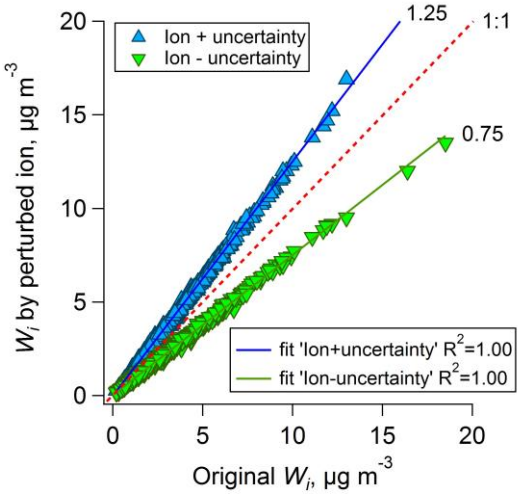

Fig. 6. W_i based on artificially perturbed ion data at upper and lower uncertainty limits is compared to W_i at base level. The slopes indicate the W_i uncertainty caused by ions.

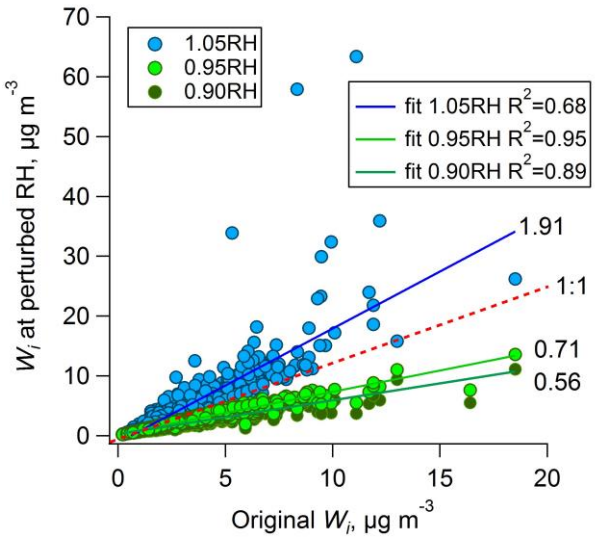

939

940 **Fig. 7.** W_i based on artificially perturbed RH at upper and lower uncertainty limits compared to W_i at base
941 level. 1.10RH (i.e., RH increased by 10%) is not plotted because it results in much larger W_i than the rest.
942 Slopes and R^2 indicate corresponding W_i uncertainty caused by variability (uncertainty) in RH.

943

944

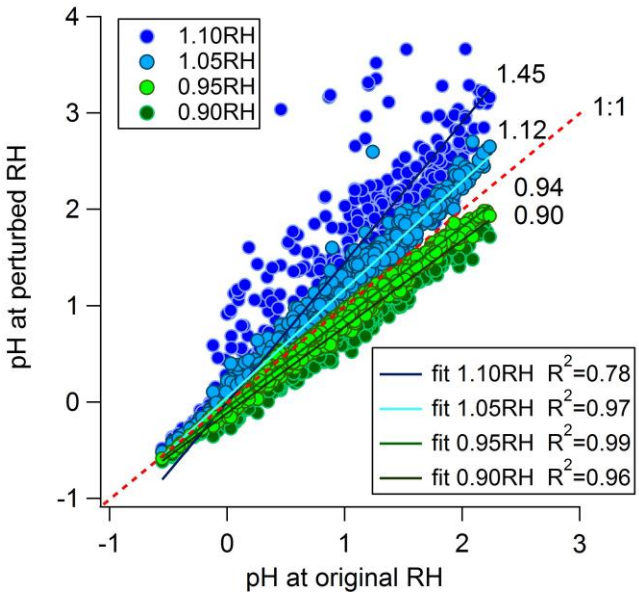

945

946 **Fig. 8.** pH predictions by perturbing RH compared to pH at base level. W_i, W_o, and H^+_{air} were
947 recalculated based on ±5% and ±10% original RH to investigate pH uncertainty. The slopes and R^2
948 indicate pH uncertainty caused by RH.

949

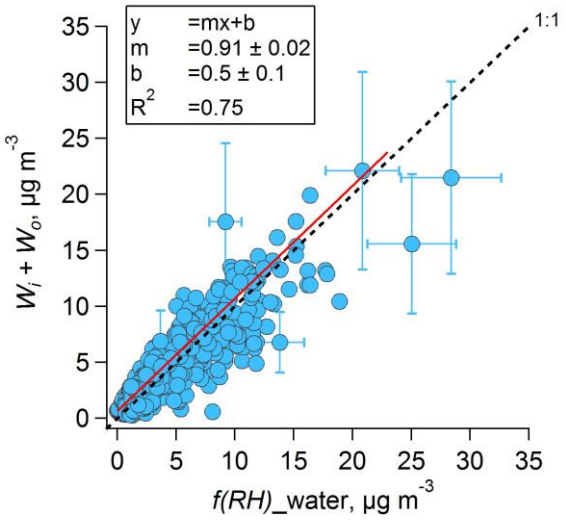

Fig. 9. Comparison between total predicted and measured water by nephelometers based on hourly averaged data at CTR (SOAS). An ODR fit was applied. Error bars for selected points are shown.

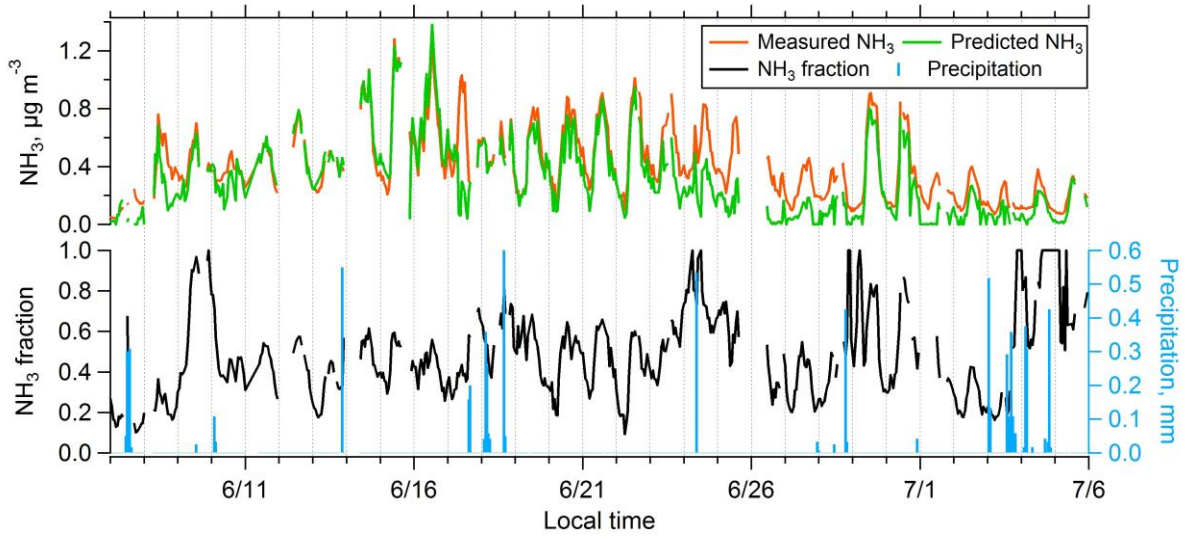

954

955 **Fig. 10.** CTR (SOAS) time series of hourly averaged measured $NH_{3(g)}$, predicted $NH_{3(g)}$, $NH_{3(g)}$ fraction
956 (i.e., measured $NH_{3(g)}/(NH_{3(g)}+NH_4^+)$) and precipitation.

957

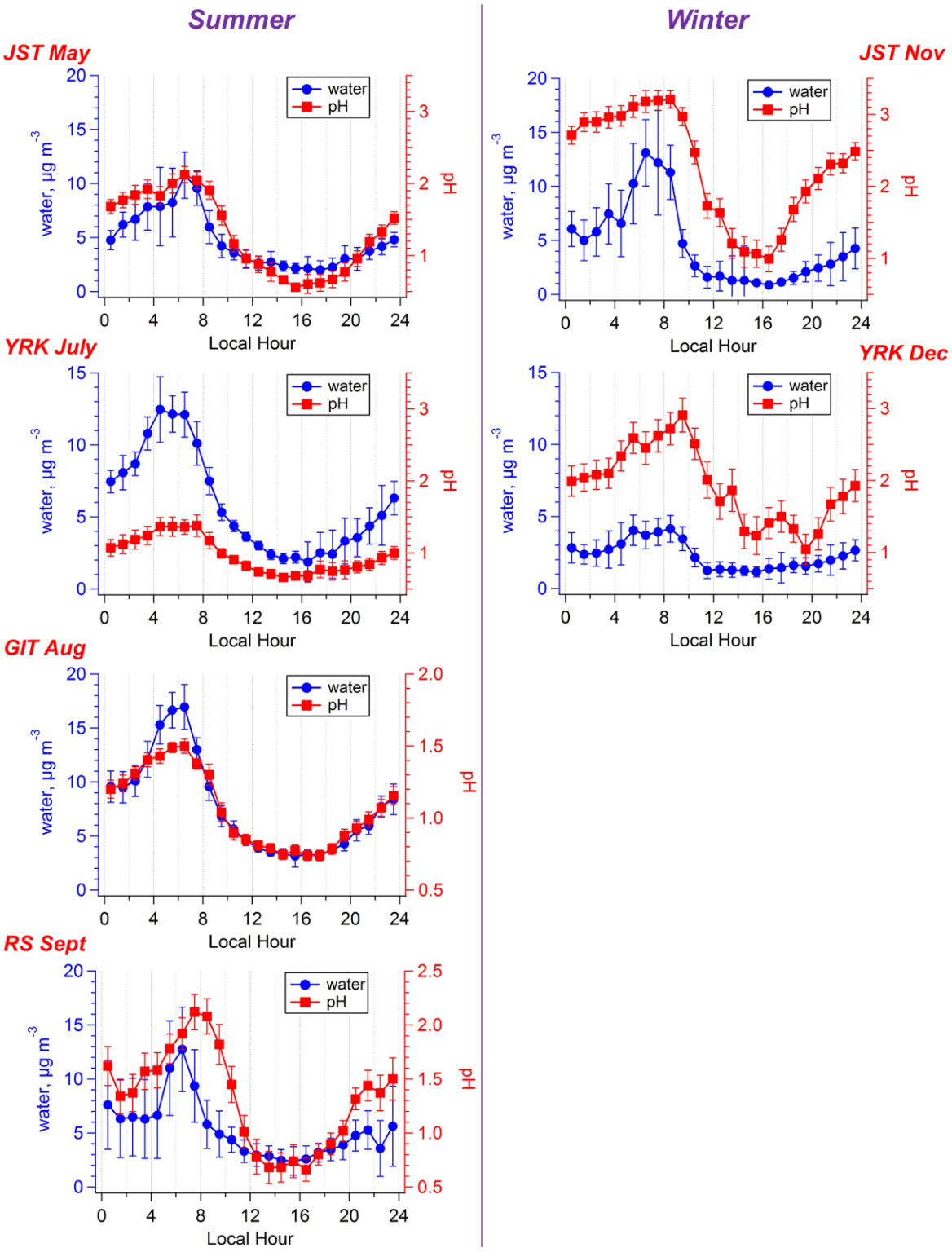

Fig. 11. LWC and pH diurnal variation at SCAPE sites: comparison between summer and winter. Median hourly averages and standard error bars at local hour are plotted. A bias correction of 1 pH unit is applied due to not considering ammonia partitioning.

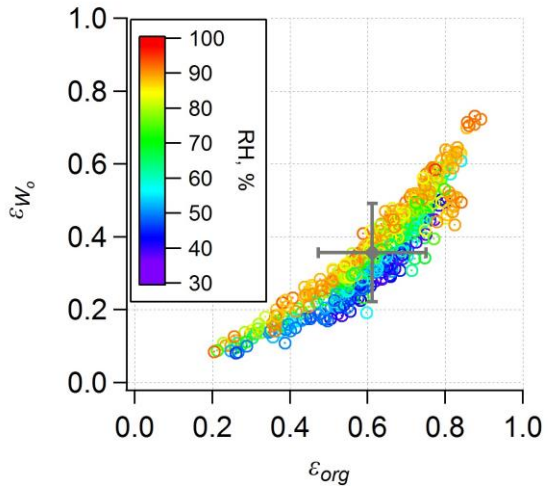

962

963 **Fig. 12.** W_o mass fraction (ε_{W_o}) plotted versus organic mass fraction at CTR (SOAS). Overall study mean

964 and standard deviation is also shown. ε_{Org} = 61 ± 14% and ε_{W_o} = 36 ± 14%.

965

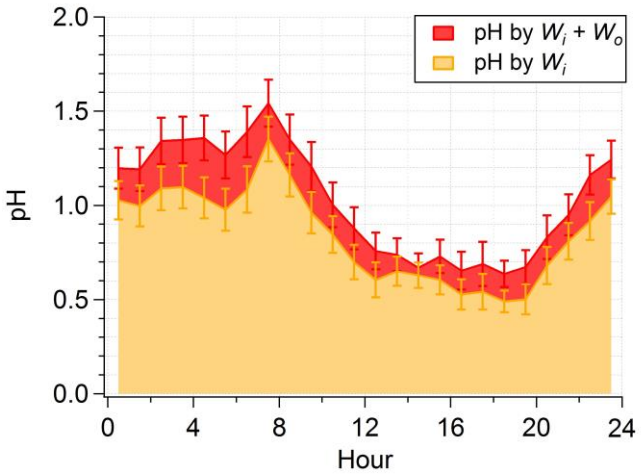

966

967 **Fig. 13.** CTR (SOAS) pH diurnal profiles based on total predicted water and W_i, respectively. Median

968 hourly averages and standard error bars at local hour are plotted.